Effects of interfacial atomic segregation and intermixing on the electronic properties of InAs/GaSb superlattices

Rita Magri
Istituto Nazionale per la Fisica della Materia e Dipartimento di Fisica, Universitá di Modena e Reggio Emilia, Modena, Italy

Alex Zunger
National Renewable Energy Laboratory, Golden, Colorado 80401

(Received 10 September 2001; revised manuscript received 27 November 2001; published 22 March 2002)

Abrupt InAs/GaSb superlattices have In-Sb and Ga-As interfacial chemical bonds that are not present in the constituent materials InAs and GaSb. We study the effect of interfacial atomic mixing on the electronic structure of such superlattices, including electron and hole energies and wave function localization, interband transition energies, and dipole matrix elements. We combine an empirical pseudopotential method for describing the electronic structure with two different structural models of interfacial disorder. First, we use the ''single-layer disorder'' model and change in a continous way the composition of the interfacial bonds. Second, we study interfacial atomic segregation using a layer-by-layer kinetic model of molecular beam epitaxy growth, fit to the observed scanning tunneling microscopy segregation profiles. The growth model provides a detailed structural model of segregated InAs/GaSb superlattices with atomic resolution. The application of the empirical pseudopotential method to such structures reveals remarkable electronic consequences of segregation, among them a large blueshift of the band gap. This result explains the surprising gap increase with growth temperature observed for similar structures. In particular we find that (i) superlattices with only In-Sb interfacial bonds have lower band gaps (by 50 meV) than superlattices with only Ga-As interfacial bonds. (ii) Heavy-hole–to–electron transition energies increase with the number of Ga-As interfacial bonds more than light-hole–to–electron transition energies. (iii) The heavy-hole $hh1$ wave functions show a strong localization on the In-Sb interfacial bonds. The heavy-hole wave functions have very different amplitudes on the Ga-As interface and on the In-Sb interface. (iv) Sb segregates at InAs-on-GaSb growth, whereas As and In segregate at GaSb-on-InAs growth, but Ga does not segregate. (v) The segregation of Sb and In induces a blueshift in the band gap. (vi) There is an in-plane polarization anisotropy due to the low symmetry of the no-common-atom InAs/GaSb superlattice. This anisotropy is reduced by interfacial segregation.

DOI: 10.1103/PhysRevB.65.165302 PACS number(s): 71.55.Eq, 73.21.−b

I. INTRODUCTION

The InAs/GaSb quantum-well and superlattice system has unusual electronic properties because of both its uncommon band alignment and its low spatial symmetry. The first unusual fact is that the band alignment of InAs/GaSb (heavy solid lines in Fig. 1) is such that the conduction band minimum (CBM) of InAs is *below* the valence band maximum (VBM) of GaSb (by ≈175 meV). Thus, $(\mathrm{InAs})_n/(\mathrm{GaSb})_n$ superlattices with thick layers ($n\to\infty$) are nominally semimetals with GaSb-like holes above the Fermi energy and InAs-like electrons below it. As the thickness of the InAs and GaSb layers decreases, quantum confinement raises the InAs-like electron level $e1$ and lowers the GaSb-like heavy-hole (hh) and light-hole (lh) levels $hh1$, $lh1$, $hh2$, etc. [Fig. 1(a)], eventually (around a period of ≈28 monolayers[1]) opening up a $hh1$-$e1$ semiconducting band gap that keeps increasing with reduced thicknesses up to ≈400 meV. This tunability of the band gap between −175 and +400 meV has made this system technologically interesting for infrared devices.[2] The second unusual fact is that, since InAs/GaSb lacks a common atomic element, this superlattice has a lower C_{2v} point group symmetry than common-atom superlattices such as InAs/GaAs or AlAs/GaAs whose symmetry is D_{2d}. The lower symmetry of InAs/GaSb is manifested by the existence of unequal bonds at the two opposite interfaces. Consider, for example, the (001) (InAs)/(GaSb) superlattice with perfectly abrupt interfaces. Since the two bulk materials GaSb and InAs do not share common atoms, the two interfaces are characterized by different bonds than the bulk In-As and Ga-Sb bonds. When growing In-As-on-GaSb (referred to as ''normal growth sequence''[3]) one finds the plane sequence (1)

$$\cdots-\mathrm{Sb}-\mathrm{Ga}-\mathrm{Sb}-\mathbf{Ga}-\mathbf{As}-\mathrm{In}-\mathrm{As}-\mathrm{In}-\cdots$$
$$(\mathrm{InAs}-\mathrm{on}-\mathrm{GaSb}) \qquad (1)$$

with the formation of a Ga-As monolayer at this interface. Analogously at the ''inverted interface'' (GaSb-on-InAs), the sequence of planes is

$$\cdots-\mathrm{As}-\mathrm{In}-\mathrm{As}-\mathbf{In}-\mathbf{Sb}-\mathrm{Ga}-\mathrm{Sb}-\mathrm{Ga}\cdots$$
$$(\mathrm{GaSb}-\mathrm{on}-\mathrm{InAs}) \qquad (2)$$

with the formation of an In-Sb monolayer at this interface. The ensuing low-C_{2v} symmetry of the ''no-common-atom'' superlattice has a number of effects on the electronic structure. We expect such unique electronic features to be sensitive to the interfacial intermixing studied here.

(i) *Coupling of lh1-hh2 and hh1-e1 at* $\mathbf{k}_\parallel=0$. Even in common-atom D_{2d} superlattices, the coupling potentials be-

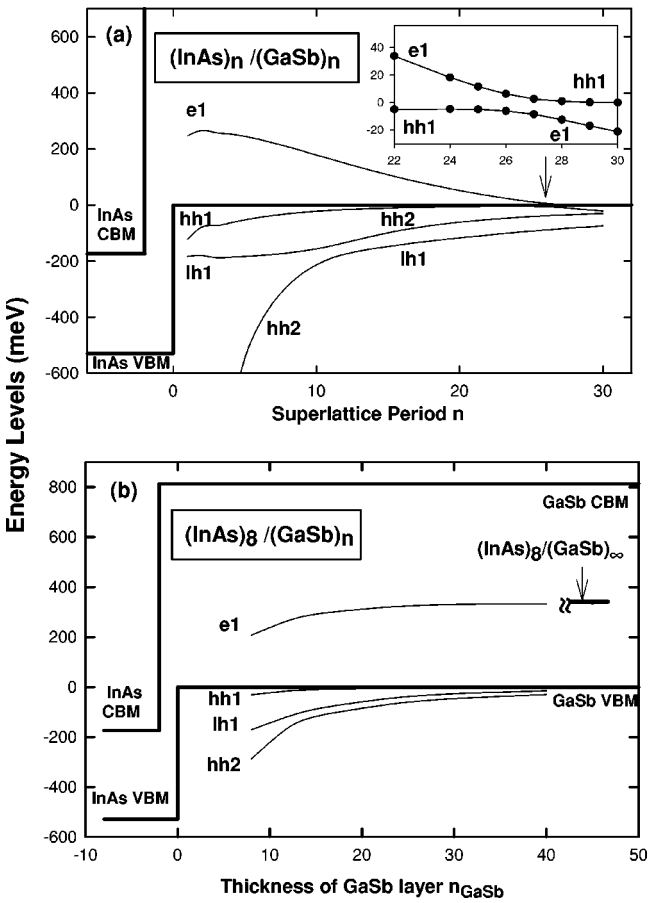

FIG. 1. First electron state $e1$ and hole states $hh1$, $lh1$, and $hh2$ vs (a) superlattice period n in symmetric $(\mathrm{InAs})_n/(\mathrm{GaSb})_n$ superlattices and (b) GaSb layer thickness n_{GaSb} in asymmetric $(\mathrm{InAs})_8/(\mathrm{GaSb})_n$ superlattices. The inset shows a close-up of the region of the $e1$ and $hh1$ anticrossing. The arrow in (a) indicates the $e1$ and $hh1$ anticrossing region, while the arrow in (b) indicates the energy of the $e1$ electron state of the $n=8$ monolayers wide InAs well between very wide (infinite) GaSb layers.

tween the first light-hole $lh1$ state and the second heavy-hole state $hh2$ and, respectively, between the first heavy-hole state and the first electron state $e1$ are already nonzero by symmetry, $V_{lh1\text{-}hh2}(\mathbf{k}_\parallel=0)\neq 0$ and $V_{hh1\text{-}e1}(\mathbf{k}_\parallel=0)\neq 0$ at zero in-plane momentum ($\mathbf{k}_\parallel=0$). Consequently, (a) if $lh1$ and $hh2$ approach degeneracy, the $lh1$ and $hh2$ levels anticross (as opposed to cross) at some critical superlattice period [$\approx$60 ML for $(\mathrm{AlAs})_n/(\mathrm{GaAs})_n$ (Ref. 4) and $\approx$15 ML for $(\mathrm{InAs})_n/(\mathrm{GaSb})_n$ (Ref. 1)]; (b) the transitions $lh1\leftrightarrow e2$ and $hh2\leftrightarrow e1$ become dipole allowed; (c) $hh1$ will anticross $e1$. In InAs/GaSb this occurs at $\approx$28 ML (Ref. 5) (see also inset to Fig. 1). (a), (b), and (c) do not occur if the coupling potentials $V_{lh1\text{-}hh2}(\mathbf{k}_\parallel=0)$ and $V_{hh1\text{-}e1}(\mathbf{k}_\parallel=0)$ are zero, as is the case in the conventional eight-band $\mathbf{k}\cdot\mathbf{p}$ model[6] which does not ''see'' the correct atomistic C_{2v} or D_{2d} symmetry, confusing it with T_d. Thus, conventional eight-band $\mathbf{k}\cdot\mathbf{p}$ models give *crossing* of $lh1$ and $hh2$, or $hh1$ and $e1$, and dipole *forbidden* $lh1\leftrightarrow e2$ and $hh2\leftrightarrow e1$ transitions.

(ii) *Coupling of lh1 and hh1 at* $\mathbf{k}_\parallel=0$. In common-atom superlattices with equivalent interfaces, this coupling vanishes at $\mathbf{k}_\parallel=0$. However, in no-common-atom superlattices with inequivalent interfaces $V_{lh1\text{-}hh1}(\mathbf{k}_\parallel=0)\neq 0$ by symmetry. Consequently, (a) if $lh1$ and $hh1$ approach degeneracy $lh1$ will anticross (as opposed to cross) $hh1$. (b) The $e1\leftrightarrow hh1$ and $e1\leftrightarrow lh1$ transitions develop an in-plane polarization anisotropy whereby the dipole transitions have unequal strength along the [110] and [$-$110] in-plane directions.[1,7,8] Effects (a) and (b) are unique to C_{2v} superlattices with inequivalent interfaces and are expected to drastically change as the superlattice interfaces are modified.

(iii) *Interfacial "spikes" in the band allignments*. Since both the ''normal'' interface and the ''inverted interface'' manifest fundamentally new types of chemical bonds (Ga-As and In-Sb, respectively) absent in the constituent binary compounds (InAs and GaSb), we expect such bonds to have their own band offsets. Pseudopotential calculations[9] indeed show considerable local variations (''spikes'') in the band offsets across these interfaces. In particular, the In-Sb strained layer has a rather high hh VBM [230 meV above GaSb (Ref. 1)] which can act as a hole trap. These interfacial potential spikes must naturally be sensitive to the interfacial composition and intermixing.

The foregoing discussion highlights the importance of studying interfacial morphology in no-common-atom superlattices, where the interfacial symmetry of abrupt structures mandates unique electronic properties. There are a number of experimental reasons to consider the interfacial morphology of such superlattices and their effects on the electronic properties. First, the known tendency[3] of Sb to surface segregate relative to As and the tendency of In to segregate relative to Ga suggests possible disorder effects on interfacial morphology. Second, recent cross-sectional scanning tunneling microscopy (STM) measurements on InAs/GaSb superlattices observed directly Sb penetration into the first few InAs monolayers.[3] Third, there are conspicuous changes in the band gaps of InAs/GaSb superlattices that are observed in samples grown at slightly different conditions. These unexpectedly large effects could arise from different interfacial morphology. For example, Yang *et al.*[10] found a 30 meV increase in the nominal 280 meV gap value for a $(\mathrm{InAs})_{5.5}/(\mathrm{In}_{0.28}\mathrm{Ga}_{0.72}\mathrm{Sb})_{10}/(\mathrm{InAs})_{5.5}/(\mathrm{AlSb})_{14}$ structure when the layer thicknesses were kept constant but the growth temperature was varied from 460 to just 500 °C. Besides having such large variations in the band gap for nominally identical structures grown by the same grower, there are large variations in band gaps of the same structure grown by different growers. These data were recently summarized by Vurgaftman and Meyer[11] (see Fig. 13 in Ref. 11) who showed that there are systematic differences between the band gaps (or, via a $\mathbf{k}\cdot\mathbf{p}$ fit, between the band offsets that yield those gaps) derived using data from different groups. In some cases they found differences as large as 100 meV for structures that are nominally quite similar. Also, the energy gaps were measured to be 25–90 meV lower in InAs/GaSb superlattices with In-Sb interfacial bonds than in structures with nominally identical thicknesses but Ga-As interfacial bonds. In particular for superlattices with nominal period $n=8$, $E_g=209$ meV and $E_g=216$ meV were measured for two different samples with only In-Sb interfaces whereas

a gap $E_g = 253$ meV was measured for a sample with only Ga-As interfacial bonds, with a difference of about 40 meV.[12]

In this paper we use a fully atomistic pseudopotential model[1,5] to study the effects of interfacial intermixing in InAs/GaSb superlattices (SL's) on their electronic properties. We study two intermixing models. In the first ''single-layer disorder'' model we continuously alter the Ga-As interface layer of the sequence of Eq. (1) and the In-Sb interface layer of the Sequence of Eq. (2) into identical interfaces, thus changing the superlattice symmetry from C_{2v} to D_{2d}. In the second ''layer-by-layer segregation'' model we simulate the molecular beam epitaxy (MBE) growth via a quantitative model fit to the cross-sectional (X) STM measured segregation profiles.[3] In both cases, we apply a plane-wave pseudopotential method to study the electronic properties before and after interfacial mixing. We find that both the bond composition at the interfacial planes and segregation have important effects on the interband transition energies and on their in-plane polarization anisotropy. We find, in particular, the following.

(i) The band gaps of superlattices of period $n=8$ with only In-Sb interfacial bonds are 50 meV lower than the gaps of analogous structures with only Ga-As interfacial bonds. This value is in good agreement with experiment.[12]

(ii) The heavy-hole–to–electron transition energies increase with the number of interfacial Ga-As bonds more than light-hole–to–electron transition energies. The trend of $lh1 \leftrightarrow e1$ transition energy with Ga-As interfacial bonds is approximately linear.

(iii) The heavy-hole wave function amplitudes are much larger on the In-Sb interfaces than on the Ga-As interfaces. The electron wave functions are, instead, more delocalized and depend less on the interfacial bonding condiguration.

(iv) Sb and In segregation induces a blueshift (as large as 50 meV) of band gaps.

(v) A strong $hh1$ wave function localization takes place at the In-Sb interfacial bonds. This localization leads to a distinct behavior of the band gap versus the interfacial bond composition and superlattice period. Both the change of the interfacial bonds and segregation alter the $hh1$ wave function localization and induce large band gap changes.

(vi) We predict that Sb segregates at the normal interface, while As and In segregate at the inverted interface. Ga atoms do not segregate in the usual temperature range (400–500 °C) at which the InAs/GaSb SL's are grown.

(vii) At low growth temperature $T_g = 400\,^\circ$C anion intermixing is larger at the normal interface than at the inverted interface, in agreement with experiment. Indium penetrates deeply into the GaSb segment and its penetration length increases with T_g. Indium segregation (and at larger T_g also As segregation) at the inverted interface cause a one monolayer (1 ML) narrowing of the InAs electron well.

(viii) The in-plane polarization anisotropy is larger for structures with mostly unequal interfacial bonds (one interface with In-Sb bonds and the other with Ga-As bonds). We predict that segregation reduces the in-plane polarization anisotropy of samples grown at temperatures higher than 400 °C.

(ix) The $hh1$-$lh1$ and $lh1$-$hh2$ band coupling strengths depend substantially on the interfacial bonding configuration. The comparison of the in-plane polarization ratios of different transitions can shed light on the nature of the interfacial bonds.

Our results [mainly those in points (i), (ii), and (iv) above] explain the large spread in band gap values found in the literature for the InAs/GaSb system.[11]

II. METHOD

Since we found the continuumlike conventional $\mathbf{k}\cdot\mathbf{p}$ method to be inappropriate for short period no-common-atom superlattices,[6,13] we use a fully atomistic approach. We solve the single-particle Schrödinger equation

$$\left[-\frac{\beta}{2}\nabla^2+\sum_{n\alpha} v_\alpha(r-R_{n\alpha})\right]\psi_i(r)=\epsilon_i\,\psi_i(r), \qquad (3)$$

where $R_{n\alpha}$ denotes the position of the nth ion of type α (=In, Ga, As, Sb). The calculation includes a spin-orbit interaction; thus, the wave functions $\psi_i(r)$ are spinors with spin-up and spin-down components. The spin-orbit nonlocal potential is calculated using the small box implementation as described in Ref. 14. For the potential v_α we do not use the local density approximation (LDA), since not only does it produce the well-known[15] LDA errors in band gaps, but also the all-important effective masses are considerably in error. Instead, we fit the screened atomic pseudopotentials $v_\alpha(\mathbf{q})$ as a function of momentum $\mathbf{q}$ to calculated and measured properties of the four underlying binaries GaSb, InAs, GaAs, and InSb and their interfaces. The properties fitted include the measured bulk band energies at high-symmetry points, measured effective masses, and LDA-calculated hydrostatic and biaxial deformation potentials of the individual (VBM, CBM) band edges, as well as LDA-calculated strained band offsets. The details of the fit are described in the Appendix[16–18] and the two figures within, where we also show how the potential works for the ternary alloys GaAsSb, GaInAs, GaInSb, and InAsSb. The atomic positions $R_{n\alpha}$ are obtained by minimizing the superlattice strain energy, modeled via the valence force field[19] (see the Appendix). The wave functions are expanded in a plane-wave basis, and the Hamiltonian matrix elements are calculated in this basis with no approximation. The Hamiltonian matrix is diagonalized via the folded spectrum method.[20]

We contrast now our method with other strain-dependent empirical pseudopotential approaches that have been proposed recently in the literature for the InAs/GaSb system.

Dente and Tilton[21] have applied the empirical pseudopotential method to study the electronic structure of InAs/GaSb SL's. The quality of the band-structure fit to bulk InAs and bulk GaSb is similar in both calculations, as are the strained band offsets (540 meV for the valence offset and 172 meV for the offset between the InAs CBM and the GaSb VBM, as compared with 529 meV and 174 meV here, respectively). There are, however, some significant differences in the methods.

(i) Dente and Tilton used a *discrete* screened potential $v_\alpha(\mathbf{G}_i)$ available only at few reciprocal lattice vectors $\mathbf{G}_i$ of the two binary compounds GaSb and InAs. Instead, we fit directly a *continous* $v_\alpha(\mathbf{q})$ to all four binary compounds (GaSb, InAs, GaAs, InSb), whose bonds are present in the superlattice (Appendix) and do not make any special assumption about the shape of the interface potential: the interfacial Ga-As and In-Sb bonds are treated individually, each bond having its own band offset with respect to its environment.

(ii) We use an explicitly strain-dependent pseudopotential $v_\alpha(\mathbf{q},\epsilon)$, whereas Dente and Tilton used a strain-independent potential $v_\alpha(\mathbf{G}_i)$ and applied slight form factor adjustments to the InAs potential to fit the band gap of the strained material. However, the strain-dependent $v_\alpha(\mathbf{q},\epsilon)$ was previously shown[22] to be crucial for correctly describing strained bonds. In fact, the Ga-As and In-Sb bonds at the interfaces of the InAs/GaSb SL differ by 14%, while the lattice mismatch of either GaAs and InSb with respect to InAs and GaSb is 6%–7%.

(iii) Dente and Tilton do not model the pseudopotential of the alloys that could exist in this system, e.g., GaAsSb, GaInAs, GaInSb, and InAsSb, whereas in our method they are explicitly described (Appendix).

The differences in the methods produces by necessity different results for the superlattices, even though the bulk compounds are described similarly. For example in the $(\mathrm{InAs})_8/(\mathrm{GaSb})_m$ superlattices we (Dente and Tilton) get gaps of 238 meV (290 meV), 281 meV (314 meV), 305 meV (326 meV), and 325 meV (338 meV) for $m=8$, 12, 16, and 24, respectively.

Another strain-dependent empirical pseudopotential method for InAs/GaSb has been recently proposed by Shaw *et al.*[23,24] The inclusion of the strain dependence in the pseudopotential form factors is conceptually similar to that used in our scheme[16] [compare Eq. (5) of Ref. 20 with Eqs. (A1) and (A3) in the Appendix], but the method is implemented differently. In our case the use of a continous momentum $\mathbf{q}$ function $v_\alpha(\mathbf{q},\epsilon)$ reduces the number of parameters that have to be fit and produces authomatically the strained form factors at all the appropriate superlattice wave vectors $\mathbf{G}_i$. Shaw *et al.*[23,24] construct, instead, the strained potential $V(\mathbf{G}_i)$ through a direct numerical interpolation between the form factors corresponding to a series of hydrostatic strains. A more significant difference between our method and that of Ref. 24, is in the description of the interfacial bonds. In our method we use specific atomic pseudopotentials to describe the Ga-As and In-Sb interfacial bonds with respect to the In-As and Ga-Sb bulk compounds (see the Appendix) We have found it essential for obtaining a good description of the alloy positive band bowings. No special treatment of the different interfacial bonds is presented in Refs. 23 and 24.

III. ABRUPT $(\mathrm{InAs})_n/(\mathrm{GaSb})_m$ (001) SUPERLATTICES

A. Symmetric $(\mathrm{InAs})_n/(\mathrm{GaSb})_n$

Figure 1(a) shows the electron $e1$ and hole ($hh1$, $lh1$, $hh2$) levels of symmetric $(\mathrm{InAs})_n/(\mathrm{GaSb})_n$ (001) superlattices as a function of n. We see that as n is reduced from infinity, the $e1$ level moves up, while $hh1$, $lh1$, and $hh2$ move down, all states becoming more and more confined within the corresponding wells. When $n<28$ the superlattices acquire a semiconducting gap with the first electron state $e1$ localized in the InAs layer and the first hole state $hh1$ localized in the GaSb layer. At $n=28$ the energy of the $e1$ level becomes lower than the energy of the hole $hh1$ state. However, the expected metallization of the system does not occur because of the opening of the anticrossing gap. The calculated anticrossing gap at $k_\parallel=0$ is $E_A^{hh1,e1}=11$ meV (inset to Fig. 1). We find a strong wave function mixing at the $hh1$-$e1$ anticrossing, in good agreement with experiment[25] and other calculations.[21]

In addition to $e1$-$hh1$ coupling and anticrossing we find also anticrossing between the hole levels $lh1$ and $hh2$ around $n=13$. For superlattice periods n close to $n=13$ the wave functions of the two hole states strongly intermix. The calculated anticrossing gap is $E_A^{lh1,hh2}=40$ meV. This causes the appearance of new transitions $lh1\leftrightarrow e2$ and $hh2\leftrightarrow e1$ in the spectra that become allowed because of this mixing.

B. Asymmetric $(\mathrm{InAs})_8/(\mathrm{GaSb})_m$

Figure 1(b) shows the electron and hole states of $(\mathrm{InAs})_8/(\mathrm{GaSb})_n$ (001) SL's vs n. While the hole states move to higher energies as the thickness n of the GaSb barrier increases, [as is the case in Fig. 1(a) for symmetric $(\mathrm{InAs})_n/(\mathrm{GaSb})_n$], we see in Fig. 1(b) that also the electron state moves to *higher* energies as n increases, opposite to Fig. 1(a). The net effect is a blueshift of the band gap.

The reason for the blueshift[26] is as follows: the energy of the $hh1$ hole state moves upward as n increases and its wave function becomes less and less confined. This effect goes in the direction of *diminishing* the fundamental gap. However, the gap *increases*, instead, because the energy of the first electron state $e1$ moves upwards as n increases, by a larger amount. This is so because the wave function of the electron state becomes more and more confined in the InAs well as the thicker GaSb layer provides a larger barrier for the electron states and diminishes the interaction between electron states in subsequent InAs wells. It is indeed the coupling between the $e1$ states of neighboring InAs wells that pushes down the energy of the $e1$ ''bonding'' electron states in superlattices with short GaSb barriers.

The calculated transition energies at Γ from the various valence subbands to the lowest conduction subband are reported in Table I, where they are compared with the values deduces from the absorbance spectroscopy results of Kaspi *et al.*[26] The comparison is only tentative, because the procedure of extracting sharp transition energies from broad absorption spectra has some uncertainties. Nevertheless, the interband transitions seen by the experiment are predicted reasonably well by our calculations, in particular the blueshift observed for the energy of the first transition when the GaSb thickness is increased. The measured samples we are comparing our calculations with in Table I have been grown with particular attention to minimize imperfections like in-

TABLE I. Calculated transition energies from the valence subbands to the lowest conduction band $e1$ compared with the experimental values of Ref. 26 (in parentheses). The assignments shown here are only tentative. We have indicated with an asterisk the transitions with a large dipole oscillator strength. For the 8/32 and 8/40 superlattices the first transition involves a mixed $lh1$ and $hh1$ hole state allowed by the C_{2v} symmetry.

InAs/GaSb (ML/ML)	$e1$-$hh1$ (meV)	$e1$-$lh1$ (meV)	$e1$-$hh2$ (meV)	$e1$-$hh3$ (meV)	$e1$-$hh4$ (meV)	$e1$-$lh2$ (meV)	$e1$-$hh5$ (meV)	$e1$-$lh3$ (meV)	$e1$-$hh6$ (meV)
8/8	238* (282)	378* (402)	494 (670)						
8/12	281* (304)	383* (381)	428* (516)						
8/16	305* (328)	378* (370)	406* (464)	539* (600)					
8/24	325* (350)	364* (364)	387* (397)	445* (487)	557 (594)				
8/32	331* (350)	355* (363)	373 (381)	404* (433)	473 (514)	552	561*	605* 621	
8/40	333* (350)	348* (362)	363 (376)	381* (409)	428* (465)	487	497	541* 536	565 606

teratomic diffusion and segregation during the growth and interfacial broadening, obtaining high-quality superlattices very close to the abrupt model, as successive characterizations have shown.[26] However, it is impossible to eliminate completely these imperfections and grow perfectly abrupt interfaces. It is then important to assess how the imperfections can modify the results we have obtained for the perfect geometry and recompare with experiment.

IV. SINGLE-LAYER MODEL OF INTERFACIAL DISORDER

A. Model

Our first model of interfacial disorder aims at transforming simply and continuously the C_{2v} system with two unequal interfaces [Eqs. (1) and (2)] to a D_{2d} system with equal interfaces. We do this as follows. We observe first that if in the plane sequence of Eq. (1) of the InAs-on-GaSb interface we change the interface As plane into a Sb plane, then we trasform the Ga-As interface into a In-Sb interface. If we leave the other interface sequence, that of Eq. (2), unchanged, we end up with a superlattice having a noninteger number of layers $(InAs)_{7.5}/(GaSb)_{8.5}$, with two *equivalent* In-Sb interfaces. We denote this configuration as $(InAs)_7$-In-Sb-$(GaSb)_8$ to stress the presence of an extra In-Sb interface. In a similar way, we can change the Sb plane at the GaSb-on-InAs interface [sequence of Eq. (2)] into an As plane, leaving the other interface, the sequence of Eq. (1), unchanged. The resulting SL has now two *equivalent* Ga-As interfaces. We indicate this $(InAs)_{8.5}/(GaSb)_{7.5}$ SL configuration as $(GaSb)_7$-Ga-As-$(InAs)_8$.

By denoting the fraction of Sb atoms at the interfacial anion plane i ($i=1$ for the normal interface, $i=2$ for the inverted interface), as $x_I^{(i)}$, we have the following.

(1) $(InAs)_8/(GaSb)_8$ [$x_I^{(1)}=0$ (Ga-As bonds) at the InAs-on-GaSb interface and $x_I^{(2)}=1$ (In-Sb bonds) at the GaSb-on-InAs interface].

(2) $(InAs)_7$-In-Sb-$(GaSb)_8$ [to $x_I^{(1)}=1$ (In-Sb bonds) at the InAs-on-GaSb interface and $x_I^{(2)}=1$ (In-Sb bonds) at the GaSb-on-InAs interface].

(3) $(GaSb)_7$-Ga-As-$(InAs)_8$ [$x_I^{(1)}=0$ (Ga-As bonds) at the InAs-on-GaSb interface and $x_I^{(2)}=0$ (Ga-As bonds) at the GaSb-on-InAs interface].

By inserting mixed $Sb_{x_I}As_{1-x_I}$ layers we can vary gradually the interfacial composition and change continuously $x_I^{(i)}$ ($0<x_I^{(i)}<1$). To generate configurations with fractional interfacial composition we use a larger surface unit cell. The interface unit cell is shown in Fig. 2. It is a 4×4 interface unit cell in the substrate plane, containing 16 primitive unit cells. In figure we show also the projection onto the (001) interface of the standard cubic unit cell. We obtain different interfacial configurations x_I by occupying differently the 16 planar sites with Sb and As atoms. Thus, all the configurations of the model considered in this section are uniquely identified by (i) the composition $x_I^{(i)}$ of the two interfacial anion planes ($x_I^{(1)}$) and ($x_I^{(2)}$) and (ii) the atomic occupation by As and Sb of the 16 sites of the interfacial unit cell (Fig. 2).

The atomic configurations of the single-layer model leave the cation sublattice unchanged with respect to the abrupt geometry. On the contrary, the global composition of Sb atoms changes with the interfacial compositions $x_I^{(i)}$. In an $n=8$ superlattice the fraction of Sb atoms varies from a maximum $x_{Sb}=0.5625$ for the configuration with two In-Sb interfaces ($x_I^{(1)}=1, x_I^{(2)}=1$) to a minimum $x_{Sb}=0.4375$ for the configuration with two Ga-As interfaces ($x_I^{(1)}=0, x_I^{(2)}=0$).

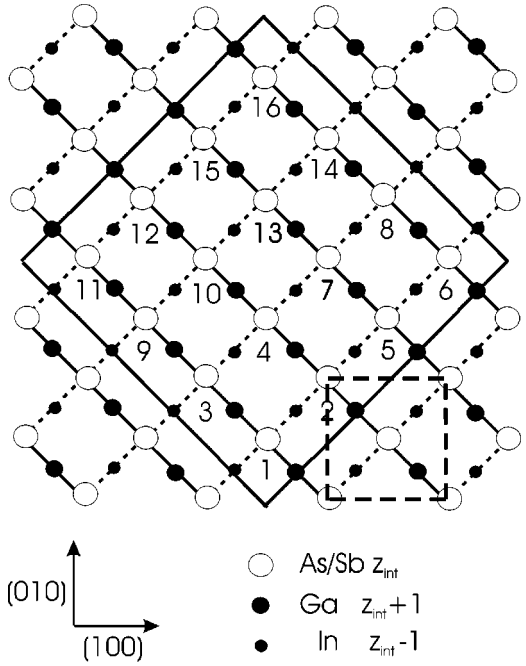

FIG. 2. Interface unit cell on a (001) plane. The 16 atomic sites are indicated.

B. Results for the single-layer model of interfacial disorder: Integer $x_I^{(i)}$

In this section we study the dependence of the superlattice band structure on the interfacial structure. We consider the three simplest cases: (a) $(InAs)_8/(GaSb)_8$ (having one Ga-As interface and one In-Sb interface), $(GaSb)_7$-Ga-As-$(InAs)_8$ (two Ga-As interfaces), and $(InAs)_7$-In-Sb-$(GaSb)_8$ (two In-Sb interfaces). In Fig. 3 we show the band structure close to the Γ point of the three upper hole bands and the lowest electron band, plotted along the in-plane [110] and [−110] directions of the Brillouin zone (BZ). Because of the D_{2d} symmetry, the band structures of $(GaSb)_7$-Ga-As-$(InAs)_8$ and of $(InAs)_7$-In-Sb-$(GaSb)_8$ are identical along the [110] and [−110] directions, while in the case of the $(InAs)_8/(GaSb)_8$ superlattice, whose symmetry is C_{2v}, the dispersion of the valence bands along the [110] direction is significantly different from that along the [−110] direction. By comparing the three band structures shown in Fig. 3 we can identify the features associated with the In-Sb interfacial bonds. The presence of the In-Sb bonds [Fig. 3(c)], leads to a *lower* band gap, changing from $E_g = 279$ meV (253 measured[12]) in the structure with two Ga-As interfaces [Fig. 3(b)] to $E_g = 229$ meV (209–216 measured[12]) in the structure with two In-Sb interfaces [Fig. 3(c)]. Another clear fingerprint of the In-Sb interfacial bonds is a larger spin splitting in both the valence and conduction bands, as shown in Fig. 3(c).

In Fig. 4 we plot the (xy-averaged) wave function amplitudes along the growth [001] direction for the three upper hole states and the lowest electron state for the same three superlattices at the BZ center. Again, as seen in panel (a) of Fig. 4, the lower C_{2v} symmetry of the $(InAs)_8/(GaSb)_8$ superlattice induces an asymmetry of the wave function with respect to the well center: larger amplitude is localized on the In-Sb interface and less on the Ga-As interface [arrows in Fig. 4(a)]. The difference is quite substantial for the heavy-hole $hh1$ and $hh2$ wave functions that are localized on the In-Sb interfacial bond. The $lh1$ and $hh2$ states of the D_{2d} superlattice [panel (c)], where two In-Sb interfaces are present, have a larger amplitude at the interfaces than in the middle of the GaSb layer. The opposite is true for the D_{2d} superlattice with two Ga-As interfaces [panel b]. Thus, the In-Sb bonds behave like local potential wells localizing holes. The electron wave functions are, instead, more delocalized and more independent of the interfacial structure.

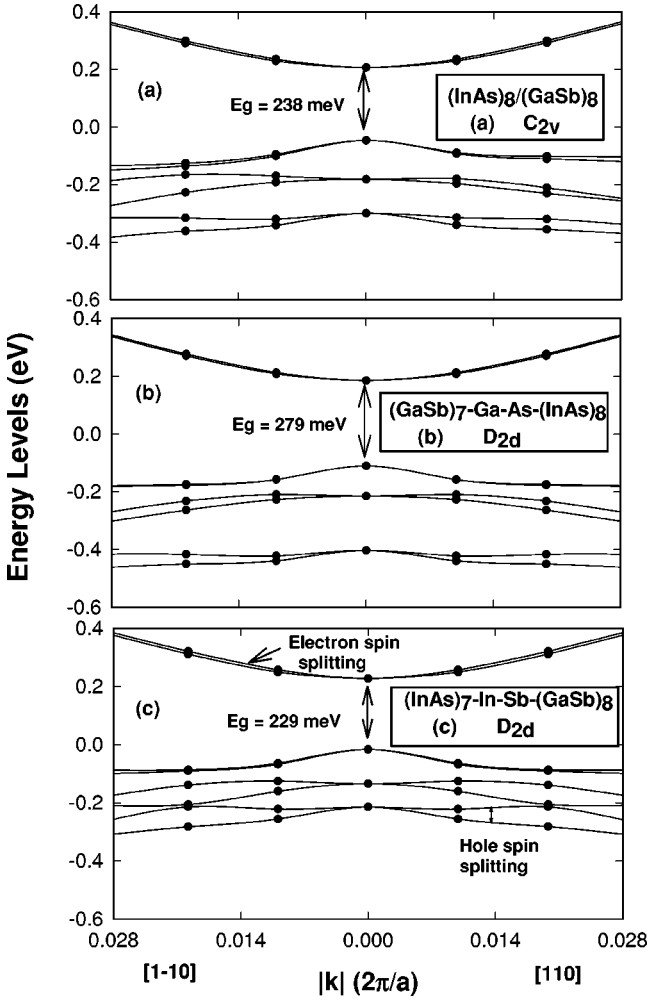

FIG. 3. Energy level dispersion for (a) $(InAs)_8/(GaSb)_8$, (b) $(GaSb)_7$-Ga-As-$(InAs)_8$, and (c) $(InAs)_7$-In-Sb-$(GaSb)_8$ superlattices along the [110] and [−110] directions of the Brillouin zone. Band gaps values E_g are indicated by arrows, as are the hole and electron spin splittings.

The above discussion referred to the BZ center. The study of the behavior of the D_{2d} symmetry $(InAs)_7$-In-Sb-$(GaSb)_8$ superlattice wave functions off-Γ shows that the hole wave functions are localized at only one of the two In-Sb interfaces when the k points lie along the [110] direction and at the other In-Sb interface when the k points lie along the [−110] direction.

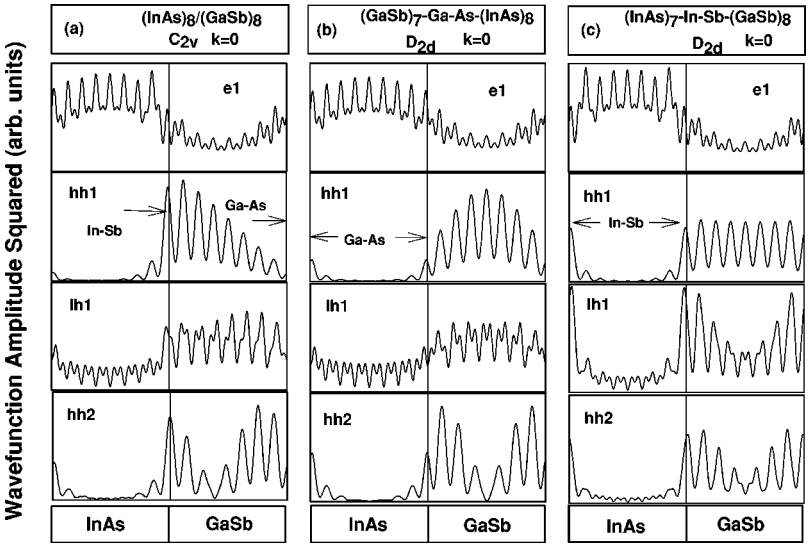

FIG. 4. In-plane averaged wave function amplitude squared of the $e1$, $hh1$, $lh1$, and $hh2$ states at the Brillouin zone center for the (a) $(InAs)_8/(GaSb)_8$, (b) $(GaSb)_7$-Ga-As-$(InAs)_8$, and (c) $(InAs)_7$-In-Sb-$(GaSb)_8$ superlattices. The arrows indicate the composition of the related interfacial bonds.

Figure 5 shows the calculated dipole transition elements of the $hh1 \rightarrow e1$ transition at $k=(0.02,0.02,0)2\pi/a$ and at $k=(-0.02,0.02,0)2\pi/a$ for the three superlattices. We can see the following: (i) the transition strengths strongly depend on the polarization of the radiation (001) vs (110) or (−110); (ii) there is a strong anisotropy between the transitions with polarization along the two in-plane directions [110] and [−110], respectively, for all the superlattices and for both k vectors; and (iii) the in-plane polarization anisotropy of the D_{2d} symmetry superlattices at $k=\alpha[110]$ is *exactly* compensated by the anisotropy at $k=\alpha[-110]$, so that the integration over the entire BZ gives a net zero anisotropy consistent with the D_{2d} symmetry. This compensation does not occur in the case of the superlattice with C_{2v} symmetry, where a residual in-plane polarization anisotropy is expected after integration over the entire BZ.

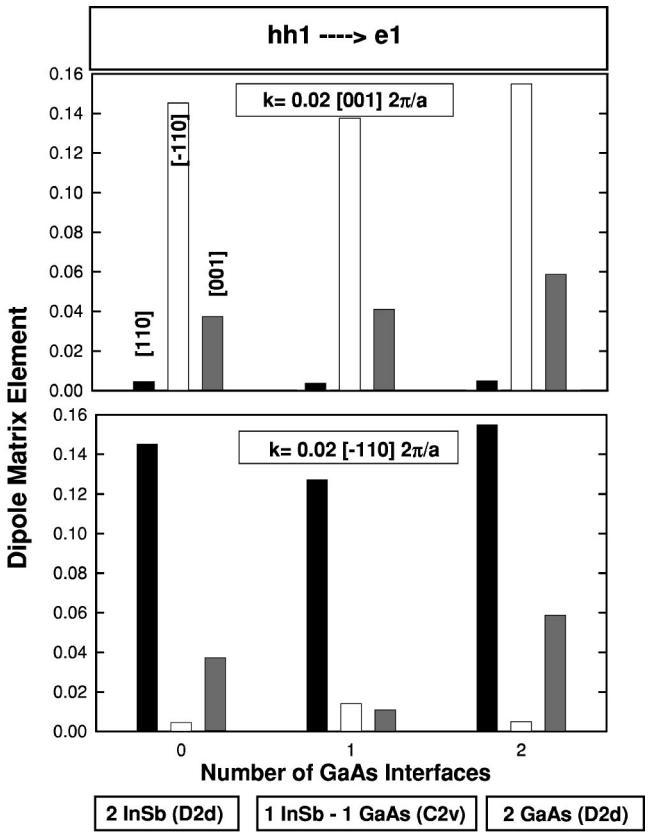

FIG. 5. Dipole matrix elements of the $hh1 \leftrightarrow e1$ interband transition for $(InAs)_7$-In-Sb-$(GaSb)_8$ (zero Ga-As interfaces), $(InAs)_8/(GaSb)_8$ (one Ga-As interface), and $(GaSb)_7$-Ga-As-$(InAs)_8$ (two Ga-As interfaces), calculated at two k points of the Brillouin zone, one along the [110] direction, the other along the [−110] direction. The dipole matrix elements are relative to different directions of the radiation polarization: [110], [−110], and [001].

C. Results for the single-layer model: Intermixed $Sb_{x_I}As_{1-x_I}$ interfaces

Figure 6 reports the energies of the $hh1 \rightarrow e1$, $lh1 \rightarrow e1$, and $hh2 \rightarrow e1$ interband transitions at the BZ center as a function of the number of interfacial Ga-As bonds or as a function of the total As content, $1-x$. For each value of As interfacial composition $1-x_I$ we average over a few in-plane configurations corresponding to different occupations of the interface plane sites (see Fig. 2). The dependence of the interband transition energies on the particular in-plane atomic configuration for the same composition x_I is small, about an order of magnitude smaller than the difference between the transition energies of superlattices with different interface composition. We see in Fig. 6 that (i) the energies of all transitions increase with the number of interfacial Ga-As bonds. (ii) While for the $lh1 \rightarrow e1$ transition the trend is approximately linear and with small slope, in the case of the transitions involving the heavy-hole states, deviations from linearity are observed and the slopes are larger: for the $hh2 \rightarrow e1$ transition the total increase of the transition energy with the Ga-As interfacial bonds is quite large, 146 meV, and for the $hh1 \rightarrow e1$ transition is only 50 meV. The smaller sensitivity of the $hh1 \rightarrow e1$ transition energy is due to the strong localization of the $hh1$ wave function at the In-Sb bonds which pins the energy of the $hh1$ level. Indeed, since the position of the electron state $e1$ moves up linearly with the

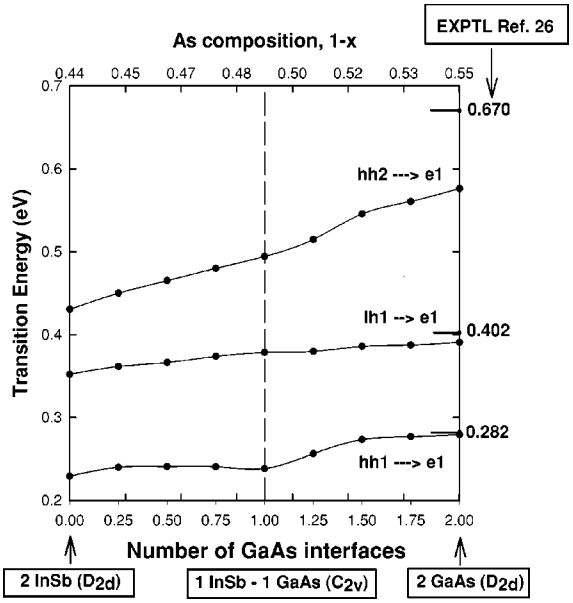

FIG. 6. Calculated energies of the first three interband transitions at the Brillouin zone center versus the number of Ga-As interfaces and the total As fraction in the superlattices. At the right end side the experimental data from Ref. 26 are given for comparison. We disagree with the assignment $hh2 \leftrightarrow e1$ of the third transition.

increase of Ga-As interfacial bonds, the behavior shown in Fig. 6 for the transition energies reflects mainly the shifts of the heavy-hole levels. (iii) While the agreement with the experiment[26] for the first two transitions is good, we disagree with the assignment of the third transition at 670 meV to $hh2 \leftrightarrow e1$. We will come back to this point again in Sec. V.

Figure 7 gives the dipole matrix elements of the $hh1 \rightarrow e1$, $lh1 \rightarrow e1$, and $hh2 \rightarrow e1$ transitions at the BZ center for polarization directions along the superlattice growth [001] axis and the two in-plane [110] and [−110] axes as a function of the number of Ga-As interfacial bonds. We can see that (1) in the case of the $hh1 \rightarrow e1$ transition, the total oscillator strength is higher for the two D_{2d} structures with zero Ga-As interfacial bonds and with two Ga-As interfaces, than for the C_{2v} structure with only one Ga-As interface.

(2) The in-plane polarization anisotropy is higher in the case of the C_{2v} superlattice. We can conclude, therefore, that a larger inequality of the interfacial bonds at the two subsequent interfaces leads to a larger in-plane polarization anisotropy.

(3) In the case of the $lh1 \rightarrow e1$ transition there is a switch in magnitude of the oscillator strengths of the [110] and [−110] polarizations and the oscillator strength is much larger for the [001] polarization than for in-plane polarization. The total (and [001]-polarized) transition probability increases with the number of Ga-As interfacial bonds.

(4) The intensity of the $lh1 \rightarrow e1$ total oscillator strength [Fig. 7(b)] is anticorrelated to that of the $hh2 \rightarrow e1$ transition [Fig. 7(c)]. The $hh2 \rightarrow e1$ transition is parity forbidden in the standard envelope function theory but it can gain some finite probability through the mixing of $hh2$ with $lh1$. [For this reason we do not believe that the observed[26] transition at 670 meV was correctly assigned to the $hh2 \rightarrow e1$ transition (see Fig. 6).] The total dipole strength of the $hh2 \rightarrow e1$ transition diminishes with the increase of Ga-As interfacial bonds. The intensity of the $hh2 \rightarrow e1$ is exactly opposite with respect to the dipole strength of the $lh1 \rightarrow e1$ transition. This means that the $lh1$-$hh2$ coupling is larger in the case of the two In-Sb interfaces than in the case of the two Ga-As interfaces. Also, for structures having an excess of In-Sb bonds at both interfaces (Sb-rich structures), the in-plane polarized $hh2 \leftrightarrow e1$ transition acquires some magnitude and a strong anisotropy between the [110] and [−110] directions (except

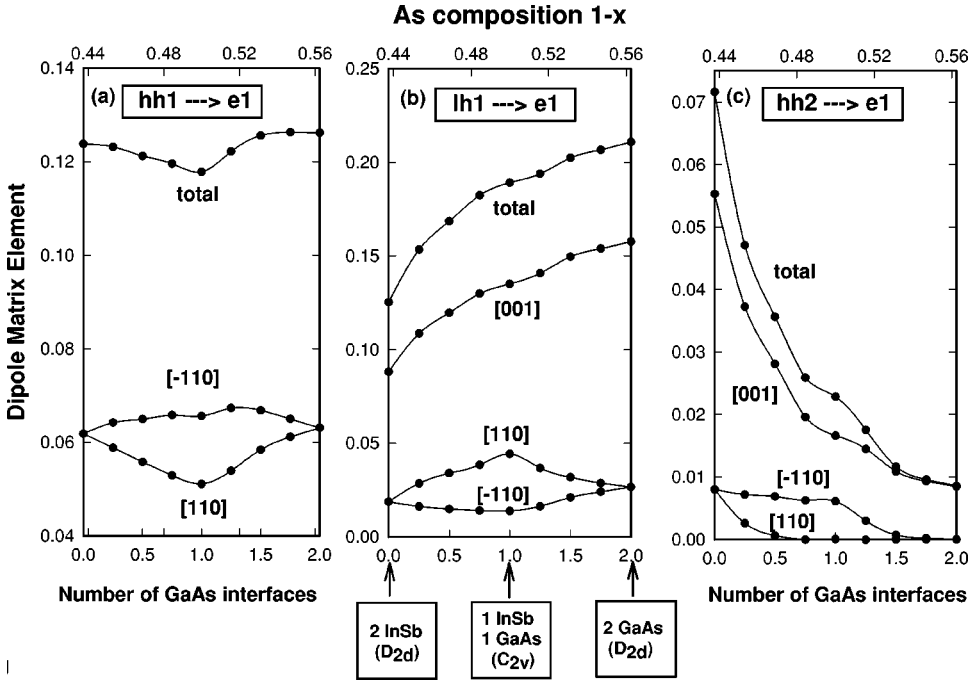

FIG. 7. Total and polarization resolved (along the [110], [−110], and [001] directions) dipole matrix elements of the $hh1 \leftrightarrow e1$, $lh1 \leftrightarrow e1$, and $hh2 \leftrightarrow e1$ interband transitions vs the number of Ga-As interfaces and the total As fraction in the superlattices.

TABLE II. Results for the in-plane polatization ratios $|\lambda_{i,j}|$ of the $hh1 \leftrightarrow e1$ and $lh1 \leftrightarrow e1$ transitions for the structures of the single-layer model. $x_I^{(i)}$ denotes the fraction of interfacial Sb atoms at interface $i=1$ (normal) and $i=2$ (inverted).

Structure	Interfacial composition		In-plane polarization ratios $\lvert\lambda_{i,j}\rvert$		
	$x_I^{(1)}$	$x_I^{(2)}$	$\lambda_{hh1,e1}$	$\lambda_{lh1,e1}$	$\lvert\lambda_{lh1,e1}\rvert$ / $\lvert\lambda_{hh1,e1}\rvert$
$(InAs)_7$-In-Sb-$(GaSb)_8$	1.00	1.00	0.000	0.000	
	0.75	1.00	0.044	0.275	6.3
	0.50	1.00	0.076	0.392	5.2
	0.25	1.00	0.109	0.464	4.3
$(InAs)_8$/$(GaSb)_8$	0.00	1.00	0.124	0.524	4.2
	0.00	0.75	0.111	0.384	3.5
	0.00	0.50	0.067	0.205	3.0
	0.00	0.25	0.030	0.088	2.9
$(GaSb)_7$-Ga-As-$(InAs)_8$	0.00	0.00	0.000	0.000	

the D_{2d} structure which has zero polarization anisotropy). This observation shows that there is a definite dependence of the $lh1$-$hh2$ band coupling on the nature of the interface bonds.

A comparison of the polarization ratios

$$\lambda_{i,j}=\frac{P_{110}^{i,j}-P_{-110}^{i,j}}{P_{110}^{i,j}+P_{-110}^{i,j}} \tag{4}$$

(where P indicates the transition dipole oscillator strength of transition $i \rightarrow j$) of the $hh1 \rightarrow e1$ and $lh1 \rightarrow e1$ transitions can also shed some light on the composition of the interfacial bonds. In Table II we give the calculated polarization ratios $|\lambda|$ of the $hh1 \leftrightarrow e1$ and $lh1 \leftrightarrow e1$ transitions for one structure for each $\{x_I^{(i)}\}$ value. We observe that the following.

(i) The polarization ratios of the $lh1 \leftrightarrow e1$ transitions are always larger than those of the $hh1 \leftrightarrow e1$ transitions.

(ii) A very small (<0.05) polarization ratio of $hh1 \leftrightarrow e1$ means that the two interfaces of the superlattice have approximately the same bonds.

(iii) A ratio between the magnitude of the polarization ratios of the $hh1 \leftrightarrow e1$ and of the $lh1 \leftrightarrow e1$ transitions, given in Table II, larger than 0.4 is an indication that the structure is Sb rich with a larger number of interfacial In-Sb bonds than of Ga-As bonds.

In this section we have seen that the nature of the interfacial bonds in the no-common-atom superlattices has a strong effect on the in-plane polarization anisotropy of the single interband transitions. We will see next that also segregation affects the energies and the in-plane polarization anisotropy of the transitions.

V. KINETIC GROWTH MODEL OF SEGREGATION

A. Model

While the single-layer model of interfacial disorder clarifies the role of the interfacial bond symmetries on the electronic structure and the interband transitions, it does not take into account the effects of atomic segregation, diffusion, and cross incorporation occurring during sample growth. To generate composition profiles for GaSb/InAs superlattices we have relied on a kinetic model for MBE growth, first introduced by Dehaese *et al.*[27] which we have extended to treat simultaneously the segregation of both group-III and group-V species in the no-common-atom quaternary GaSb/InAs system. The model simulates a layer-by-layer growth starting from a given substrate, and, at each interface, segregation is determined by atomic exchanges between the surface layer and the first subsurface layer, for each sublattice (cation and anion) separately. Layer growth is driven by the impinging atomic fluxes with deposition rates Φ_{In}, Φ_{Ga}, Φ_{Sb}, and Φ_{As} (in ML/s). Atomic exchanges require overcoming energetic barriers for bulk-to-surface ($b \rightarrow s$) and surface-to-bulk ($s \rightarrow b$) atomic swaps. For the cation system we have the barrier $E_{In/Ga}^{b \rightarrow s}$, for subsurface In to exchange with surface Ga, and $E_{In/Ga}^{s \rightarrow b}$, for surface In to exchange with subsurface Ga. Similarly, we have $E_{Sb/As}^{b \rightarrow s}$ and $E_{Sb/As}^{s \rightarrow b}$ with similar meanings. The segregation driving forces are proportional to

$$\Delta_{In/Ga}=E_{In/Ga}^{s \rightarrow b}-E_{In/Ga}^{b \rightarrow s},$$

$$\Delta_{Sb/As}=E_{Sb/As}^{s \rightarrow b}-E_{Sb/As}^{b \rightarrow s}. \tag{5}$$

Here $\Delta_{In/Ga}>0$ (<0) implies In (Ga) segregation to the surface, whereas $\Delta_{Sb/As}>0$ (<0) implies Sb (As) segregation. The rates of $i=b \rightarrow s$ or $i=s \rightarrow b$ exchange reactions at growth temperature T_g are $P_i=\nu_i \exp(-E_{\alpha/\beta}^i/k_B T_g)$, where k_B is the Boltzmann constant and ν_i is the effective hopping frequency for which we use the commonly accepted value of 10^{13} s^{-1} for III-V compounds.[27,28] Denoting by A and B the two different kind of atoms in one sublattice (e.g., In and Ga), the rate of change of the concentration, $x_A(t)$, of surface-A atoms is given by[27]

$$\frac{dx_A^s(t)}{dt}=\Phi_A+P_1\,x_A^b(t)\,x_B^s(t)-P_2\,x_A^s(t)\,x_B^b(t). \tag{6}$$

Here $x_A^{s,b}(t)$ and $x_B^{s,b}(t)$ are the time-dependent concentrations of A and B at the surface or bulk, the first term Φ_A is the deposition rate of A atoms onto the surface, the second term is the rate of A atoms arriving from subsurface to the surface after exchanging with surface B atoms, and the last

term is the rate of A atoms leaving the surface after exchanging with bulk B atoms. The conservation of A atoms and of the total number of surface atoms at any time t leads to the conditions

$$x_A^s(t)+x_A^b(t)=x_A^s(0)+x_A^b(0)+\Phi_A t, \tag{7}$$

$$x_A^s(t)+x_B^s(t)=x_A^s(0)+x_B^s(0)+(\Phi_A+\Phi_B)t, \tag{8}$$

and, at any t, we have $x_A^b(t)+x_B^b(t)=1$. A small fraction x_0 of the segregating Sb specie is incorporated into each InAs layer during the growth because of an unwanted vapor bachground. This cross incorporation has been taken into account modifying slightly the fluxes Φ_{As} and Φ_{Sb} during the growth of InAs so as to have the incorporation of a small constant Sb fraction $x_0=0.015$ into each InAs layer, as proposed in Ref. 3. Our approximations are the following: (i) the barrier energies, Eq. (5), for atomic exchanges are assumed to be independent of the atomic species surrounding the exchanging atoms, (ii) surface reconstructions during growth are neglected, and (iii) surface roughness and the lateral disorder related to steps are also neglected.

We solve numerically Eqs. (6)–(8) for $A=$Ga, In, As, and Sb. The input to the simulation consists of growth temperature T_g, atomic fluxes Φ_α, $\alpha=$Ga, In, As, and Sb, and the four exchange energies appearing in Eq. (5). The two exchange energies for cation $E_{In/Ga}^i$ are taken as the values proposed in previous papers[27]: $E_{In/Ga}^{b\to s}=1.8$ eV and $E_{In/Ga}^{s\to b}=2.0$ eV; thus, $\Delta_{In/Ga}>0$ correctly implies In segregation. No values for $E_{Sb/As}^{b\to s}$ and $E_{Sb/As}^{s\to b}$ have been previously reported in the literature, so we fix them by fitting the growth model to the experimental Sb concentration profiles measured via cross-sectional STM (Fig. 4 of Ref. 3). The fit was described in Ref. 29 and gives $E_{Sb/As}^{b\to s}=1.68$ eV and $E_{Sb/As}^{s\to b}=1.75$ eV. Our determined $\Delta_{Sb/As}>0$ correctly shows that Sb segregates into the InAs layer, as observed.[3] $E_{Sb/As}^{b\to s}$ and $E_{Sb/As}^{s\to b}$ are both smaller than $E_{In/Ga}^{b\to s}$ and $E_{In/Ga}^{s\to b}$, so at very low growth temperatures (<375 °C) only anion segregation will be important, whereas appreciable In segregation is expected at higher temperatures (>375 °C).

The As profile at the inverted interface has been investigated by Harper *et al.*[30] In Fig. 8 we compare the As profile in GaSb predicted by the kinetic growth model at the inverted interface with the experimental As profile from Ref. 30 (dots). The growth temperature used in the model is the same (440 °C) at which the sample studied in Ref. 30 was grown. We find that the profile is not very sensitive to the the deposition rate in the range from 0.4 to 0.7 ML/s. The small As cross incorporation during GaSb growth has been taken into account. From cross-sectional STM on (110) surfaces one can see only every other layer of the anion sublattice. This is taken into account in Fig. 4 of Ref. 30 where the experimental profile is plotted versus the number of lattice constants along [001], each lattice constant corresponding to two anionic planes. However, the *origin* of the sequence is not known. Thus, in Fig. 9 we plot the calculated As profile using two possible origins: (a) the first anion plane and, separately, (b) the second anion plane from the interface (considered inthe middle of the In-Sb interfacial bonds). Both planes correspond indeed to the interface plane of Ref. 30. The second case has better agreement. We can see the following.

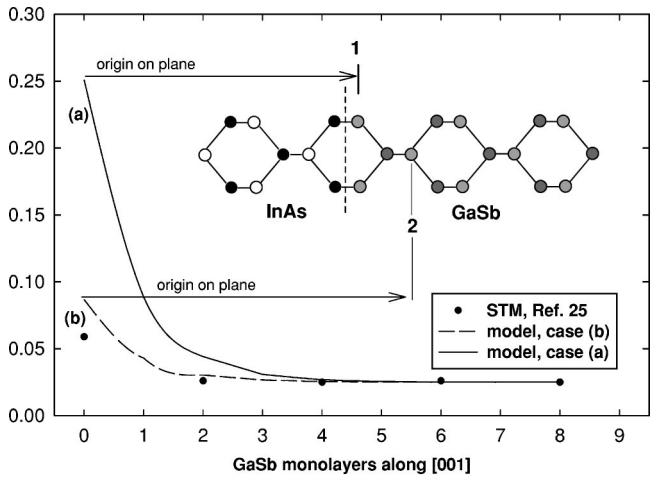

FIG. 8. Sb and Ga composition profiles along the superlattice growth direction for a $(InAs)_8/(GaSb)_8$ superlattice grown at three different temperatures: 375 °C, 450 °C, and 525 °C. The segregated profiles (diamond plus solid line) are compared in (a) and (b) with the profile of the superlattice with abrupt interfaces (dashed lines).

(i) Our segregation model predicts an As excess at the interface plane. The observed excess, therefore, can be explained as a result of anion interfacial segregation. In contrast, Harper *et al.*[30] suggested that the excess originates from exchange of surface As by Sb from the vapor. Since the initial configuration has only As in the subsurface layer and the incoming Sb atoms on the surface, segregation favors the anion exchanges that bring As onto the surface and Sb to the subsurface layer [see Eq. (6)]. Obviously this process implies the simultaneous exchange of As atoms with Sb atoms in the last InAs layer.

(ii) The As profile is predicted correctly to have a steep decrease to the bulk defect concentration, unlikely the Sb profile at the normal interface.

A new set of measurements[31] of the As profile at the inverted interface has been recently performed on the $(InAs)_8/(GaSb)_m$ samples of Ref. 26. They give 3.6% As in the first layer of GaSb, 1.1% As in the second layer, and 0.0% As in the following layers. Our model of MBE growth at $T_g=380$ °C and a deposition rate of 1 ML/s gives 10.7% As in the first layer, 1.1% As in the second layer, and 0.1% As in the third layer. Again, apart for the first layer, our predicted profile is in reasonable agreement with experimental data. The deviation found for the first (interfacial) layer can be due to other mechanisms, such as surface reconstruction or interaction with the vapor phase, which take place during the growth interruption and are not described by the present model.

B. Superlattice segregation profiles

Having obtained the segregation parameters for the InAs/GaSb system, we next model the atomistic structure of the superlattices used for optical studies.[26] We consider (001) $(InAs)_8/(GaSb)_{16}$ and $(InAs)_8/(GaSb)_8$ superlattices, lat-

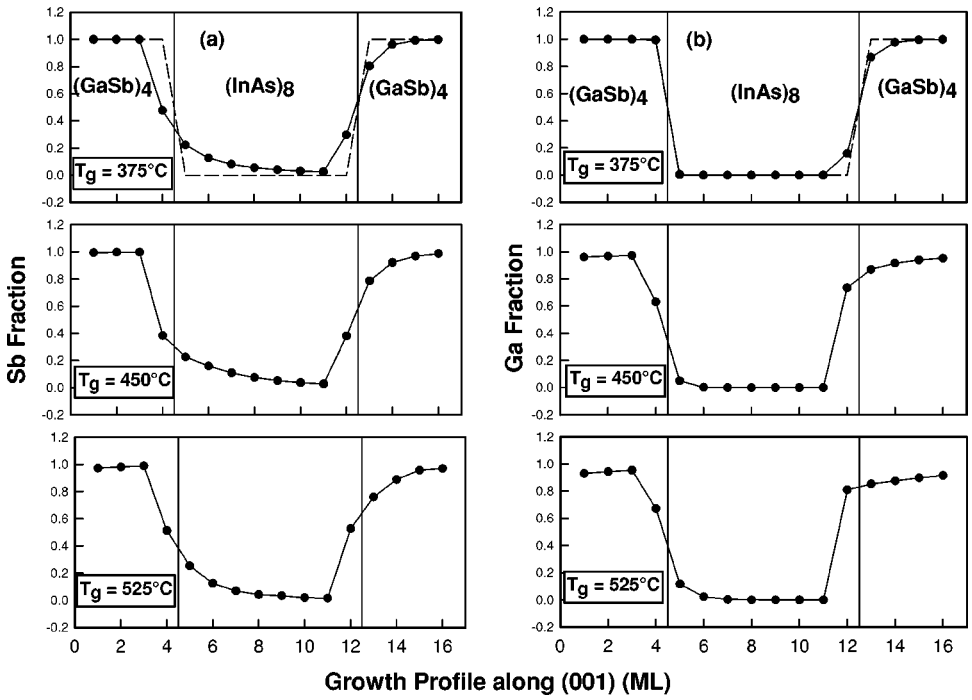

FIG. 9. As concentration profile within GaSb vs distance from the inverted GaSb-on-InAs interface in GaSb monolayers. Dots, STM result of Ref. 30; lines, results of the growth model. Cases (a) and (b) are explained in the text. Arrows show what plane in GaSb has to be considered plane zero.

tice matched to a GaSb substrate. While we have modeled the profile along the [001] growth direction no experimental information is available on the atomistic arrangement in the perpendicular substrate (001) plane. We thus assume random arrangements in these planes, consistent with the planar composition profile dictated by the growth model. To represent a fractional atomic composition we use the surface unit cell of Fig. 2 containing 16 atoms in the (001) plane, which are distributed randomly. Once we determine the superlattice configuration consistent with the solution of the growth model at a given growth temperature T_g, we permit local atomic displacements by a valence force field (VFF) approach[19] (see the Appendix).

The calculated anion and cation segregation profiles show the following general trends.

(i) Segregation leads to the penetration of Sb and In deeply into the InAs and GaSb layers, respectively. The penetration length increases with growth temperatures. At $T_g = 525\,^{\circ}\mathrm{C}$, Sb penetrates 5–6 ML into InAs, while the In penetration length is much larger (because of the larger $\Delta_{In/Ga}$), being about 11 ML.

(ii) Sb segregation occurs primarily at the normal interfaces (InAs-on-GaSb) where in the abrupt geometry a Ga-As bond exists, while In segregation occurs at the inverted interface (GaSb-on-InAs), where in the abrupt geometry an In-Sb bond exists. Our profiles at low (400 °C) growth temperatures closely agree with the STM images of the anion sublattice of Ref. 3 where it is seen that the anion intermixing is much larger at the normal interfaces than at the inverted interfaces. This result is in agreement with many experimental findings.[3,32,33]

(iii) There is also a substantial minority anion intermixing at the inverted interface and a (smaller) cation intermixing at the normal interface. This is related to the difference $\Delta_{In/Ga}$ and $\Delta_{Sb/As}$ between the barrier energies [Eq. (5)]. If Δ is small, the segregation of the specie with a higher-energy barrier (i.e., As) becomes noticeable at high T_g. We find $\Delta_{Sb/As} = 70$ meV, while $\Delta_{In/Ga}$ is much larger, 200 meV. This explains why at high T_g the anion profile at the inverted interface is more broadened (for As segregation) than the analogous cation profile at the normal interface (no Ga segregation). We will see below that segregation at the *inverted interface* leads to a narrowing of the InAs well.

In treating short-period superlattices some care has to be used, since at high growth temperatures, ($T_g > 425\,^{\circ}\mathrm{C}$), In penetrates so deeply into the GaSb layer (about 11 ML) that it reaches the next InAs layer. To treat the situation of strong segregation in short-period superlattices, we have simulated the growth of long structures with many repeated periods. Analyzing the profile of the entire structure we have found that apart from the very first one, all the other replicas have the same profile. It is this common profile that has been considered for short-period SL's. As an example, we report in Fig. 8 the anion and cation segregation profiles of $(\mathrm{InAs})_8/(\mathrm{GaSb})_8$, grown at three different temperatures: $T_g = 375\,^{\circ}\mathrm{C}$, 450 °C, and 525 °C. We can see from the Ga profile the progressive shift with T_g of the first Ga plane backward inside the InAs well at the inverted (GaSb-on-InAs) interface. This is due to the large difference $\Delta_{In/Ga}$. At high T_g, when the first Ga atomic layer is deposited onto the InAs surface, almost all the Ga atoms exchange their position with the In atoms in the layer below. These In atoms are progressively pushed forward until, ultimately, they reach the next interface, the InAs-on-GaSb normal interface. A similar substitution of the last As plane of InAs with an higher (with T_g) fraction of Sb atoms occur at the same inverted interface. The mechanism here is different and it is due, instead, to As segregation which is made possible by the small value of $\Delta_{Sb/As}$. Thus, we can see that the combination of a large

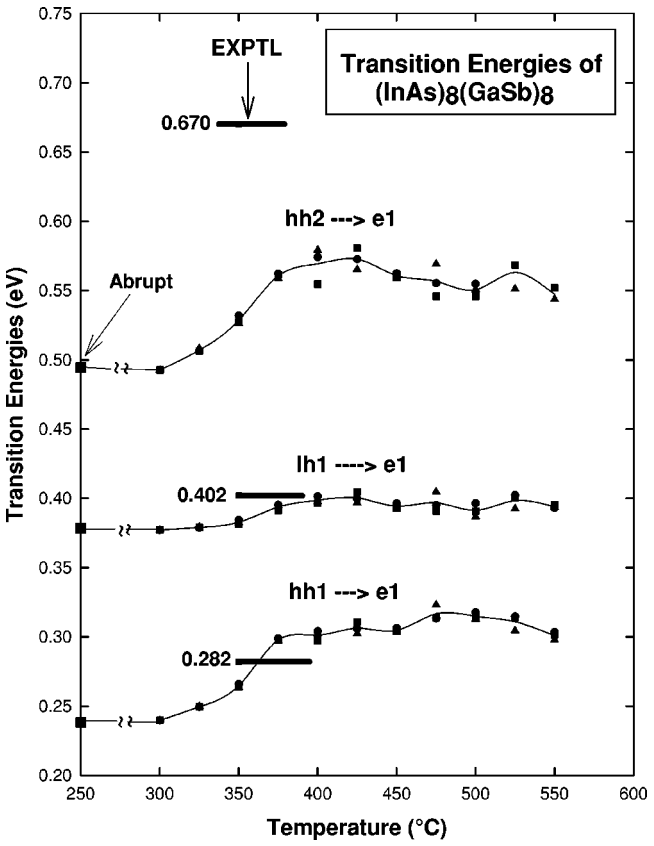

FIG. 10. Energies of the first three interband transitions at the BZ center of segregated $(InAs)_8/(GaSb)_8$ superlattices vs growth temperature. The energies from absorbance spectroscopy data from Ref. 26 are shown with horizontal bars. The dark shaded areas outline the range of the fluctuations due to the different atomic arrangements in the planes orthogonal to the growth direction correspondent to the same planar atomic composition.

$\Delta_{In/Ga}$ for cation segregation and a small $\Delta_{Sb/As}$ for anion segregation causes the narrowing of the InAs electron well with increasing T_g.

C. Results for the electronic and optical properties of segregated superlattices

In this subsection we analyze the consequences on the electronic and optical properties of the segregation-induced modification of the superlattice profile along the growth direction.

In Ref. 29 we studied the implications of segregation on the wave functions. In that paper we compared the amplitudes of the $hh1$ hole wave functions of the $(InAs)_8/(GaSb)_{16}$ superlattice for the abrupt geometry and for the structure grown at $T_g=525\,^\circ$C. The amplitude of the $hh1$ wave function, which is much larger on the In-Sb (inverted) interface than on the Ga-As (normal) interface in the abrupt geometry [see Fig. 4(a)], is substantially reduced by segregation. The wave function amplitude becomes similar at the two interfaces. Segregation affects to a lesser degree also the $lh1$ and $e1$ wave functions, which remain closer to the abrupt case (see Fig. 4).

Figure 10 shows the interband transition energies as a function of the superlattice growth temperature for the $(InAs)_8/(GaSb)_8$ superlattice. At the far left we have reported the calculated energies of the abrupt superlattice by squares, while the experimental absorbance data of Kaspi *et al.*[26] are shown with thick horizontal bars. For each growth temperature (and, thus, for the same segregation profile along the growth direction) we have calculated three structures which differ only for the in-plane atomic arrangement. We see that the following.

(1) A segregation-induced steep *increase* (blueshift) of the interband transition energies with growth temperatures takes place in the range from $T_g=300\,^\circ$C until $T_g=425\,^\circ$C. The blueshift is larger for the interband transitions involving the heavy-hole states. It is due to the narrowing of the InAs well (for electrons) and the broadening of the GaSb well (for holes) with In segregation. The electron state becomes more confined with the increasing T_g, whereas hole states become less confined, but their energies change at a smaller rate, so interband energies increase with T_g. This result explains the surprising gap increase with T_g previously observed for similar structures.[10]

(2) At $T_g>425\,^\circ$C the blueshift is reduced due to a diminishing of Sb and to a lesser extent In segregation, because of the competing segregation of As and Ga. This leads eventually to a slight decrease of the interband transition energies at the highest growth temperatures.

(3) The transition energies are generally higher than those calculated for the abrupt geometry. Only at the very low growth temperature of 300 °C do we recover the abrupt values.

(4) Segregation improves the agreement (already good) between the calculated $hh1\rightarrow e1$ and $lh1\rightarrow e1$ transition energies with the experiment. The model predictions are consistent with the fact that the samples studied in Ref. 26 have been grown at low temperature. The highest transition, which has been attributed by Ref. 26 to the $hh2\rightarrow e1$ transition, is too high and we suspect the attribution to $hh2\leftrightarrow e1$ (Ref. 26) is not correct. The $hh2\rightarrow e1$ transition has a small total dipole oscillator strength [see Fig. 7(c)]; thus, it is possible that the transition seen experimentally has another source (impurity or a higher-lying transition).

(5) At low growth temperatures, where the interfacial atomic segregation is small and there is no interfacial broadening, the transition energies do not depend greatly on the planar atomic arrangements. The difference among the transition energies corresponding to different in-plane configurations becomes larger when the superlattice growth temperature increases and, for $T_g>400\,^\circ$C, for $hh1\leftrightarrow e1$, the fluctuations can be about 10 meV, of the same order of the differences due to different values of the growth temperature in this temperature range.

Figure 11 shows the dipole transition element versus growth temperature of the $hh1\rightarrow e1$ and the $lh1\rightarrow e1$ transitions at the Brillouin zone center of the $(InAs)_8/(GaSb)_8$ superlattice. It is interesting to note the behavior of the in-plane polarization anisotropy. It increases with growth temperature until 400 °C, then it diminishes for $400\,^\circ\text{C}<T_g<525\,^\circ$C, and, finally, it increases again at $T_g>550\,^\circ$C. In

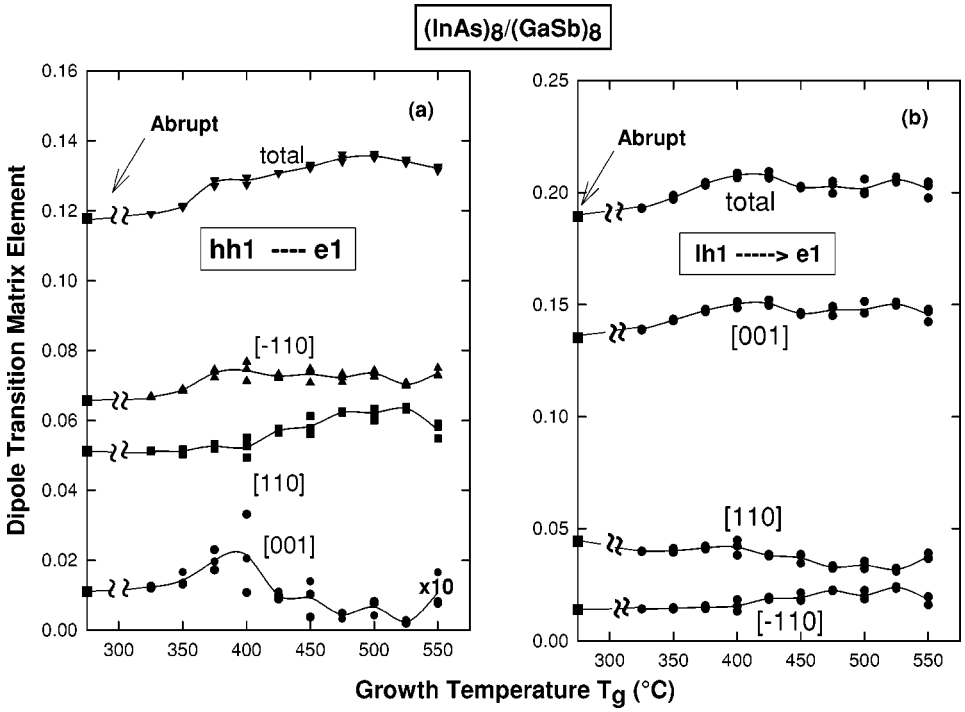

FIG. 11. Total and polarization resolved (along [110], [−110], and [001]) dipole matrix elements of the $hh1 \leftrightarrow e1$ and $lh1 \leftrightarrow e1$ transitions as a function of the superlattice growth temperature.

the case of the $hh1 \rightarrow e1$ transition [Fig. 11(a)] this trend is strictly related to the increase and decrease of the [001]-polarized component of the transition (which has a very small probability). In fact the [001] component increases when the polarization anusotropy increases. Both effects are the sign of the interface-mandated coupling (possible only in C_{2v} symmetry) between the $hh1$ and $lh1$ states. The total dipole oscillator strength of the $hh1 \rightarrow e1$ transition is larger for the segregated configurations than for the abrupt one and increases until $T_g = 500\,^{\circ}\mathrm{C}$. Also the total transition probability of the $lh1 \rightarrow e1$ transition increases with segregation until 425 °C, while, correspondingly, the transition probability of the (parity forbidden) $hh2 \rightarrow e1$ transition (not shown) diminishes. Recalling that a finite probabilty of $hh2 \rightarrow e1$ is due to the coupling of $hh2$ with $lh1$, we see that segregation diminishes the $lh1$-$hh2$ coupling.

The interband transition energies and dipole oscillator strengths at the Brillouin zone center have been calculated as a function of the growth temperature also for the $(\mathrm{InAs})_8/(\mathrm{GaSb})_{16}$ superlattice, showing an identical behavior. Thus, the trend with the growth temperature of the fundamental gap (the $hh1 \rightarrow e1$ transition) for the two $(\mathrm{InAs})_8/(\mathrm{GaSb})_8$ and $(\mathrm{InAs})_8/(\mathrm{GaSb})_{16}$ superlattices does not depend strongly on the GaSb layer thickness.

VI. SUMMARY

In this paper we have studied the effects of interfacial intermixing and segregation in InAs/GaSb superlattices on their electronic properties. We have combined an empirical pseudopotential scheme for band-structure calculations with two different structural models of interfacial disorder. With the first one, the single-layer disorder model, we have investigated the effects of the interfacial bond composition on the electron and hole wave functions and energies and on the in-plane polarization anisotropy of the single-particle interband transitions. We have found the following.

(1) The hole wave function amplitudes are larger on the In-Sb than on the Ga-As interfacial bonds.

(2) The transition energies of the superlattices having In-Sb interfacial bonds are lower than those of superlattices having only Ga-As interfacial bonds. The difference is 50 meV for the $lh1 \leftrightarrow e1$ transition in period $n = 8$ superlattices.

(3) The dipole oscillator strengths and in-plane polarization anisotropy of the interband transitions have a definite dependence on the nature of the interfacial bonds. The in-plane polarization anisotropy magnitude of the interband transitions is related to the magnitude of the heavy–light-hole couplings which depend on the kind of interfacial bonds. Thus, the simultaneous analysis of the intensity and anisotropy of the first three interband transitions could be used to characterize the nature of the interfacial bonds.

With the second model, the kinetic model of MBE growth, we have studied the effects of atomic segregation on the electronic properties. We have fit the model to the observed STM profiles to extract the segregation parameters for the InAs/GaSb system. From this procedure we have found the following.

(1) Sb and In are the segregating species.

(2) The segregation energy of In is much larger than that of Sb.

By applying the growth model we have obtained the superlattice segregation profile as a function of the growth temperature T_g. Then, we have simulated the detailed atomistic structure of the superlattices consistent with the calculated profiles. Our results show the following.

(1) Anion intermixing and interface broadening (about 2 or 3 ML) take place at the normal interface.

(2) In penetrates deeply into GaSb. The penetration length increases with growth temperature. At 525 °C it is about 11

ML. Because of the anion smaller segregation energy, the penetration length of Sb into InAs is much smaller.

(3) The inverted interface is less broadened but In and, at a larger growth temperature, As segregation leads to a 1 ML shift of the interface backward into the InAs well. As a consequence the InAs electron well becomes 1 ML narrower.

Finally, we have studied the consequences of the changes in the superlattice profiles and of the interfacial disorder on the electronic properties, applying the empirical pseudopotential method. We have found the following.

(1) A large blueshift of band gaps with increasing growth temperature. We have calculated a 50 meV gap increase for superlattices with InAs wells $n=8$ monolayers wide. The blueshift is due to an increase of the confinement energy both of the electron (because of the 1 ML narrowing of the InAs well) and of the heavy hole (whose energy gets unpinned since its amplitude on the In-Sb interfacial bonds diminishes). This result is qualitatively in agreement with the 30 meV band gap increase observed in $(InAs)_{5.5}/(In_{0.28}Ga_{0.72}Sb)_{10}/(InAs)_{5.5}/(AlSb)_{14}$ superlattices when $T_g > 450\,^{\circ}C$.[10]

(2) The in-plane polarization anisotropy remains large (equal or even larger than that relative to the abrupt geometry) until $T_g = 400\,^{\circ}C$, then becomes smaller in samples grown at higher temperatures.

ACKNOWLEDGMENTS

The work of R.M. was supported by the Italian MURST Project No. COFIN99 and by the European INTAS-99-15, whereas the work of A.Z. was supported by DOE-OS-DMS, condensed matter physics.

APPENDIX THE PSEUDOPOTENTIALS AND THE VALENCE FORCE FIELD

The crystal potential is written as a superposition of atomic potentials v_α centered on the atomic positions. We determine the atomic screened pseudopotentials $v_\alpha(\mathbf{q})$ as a function of momentum $\mathbf{q}$, for the atomic species α=Ga, Sb, In, As of the quaternary GaSb/InAs system, by fitting a large number of measurable properties. We use for the screened pseudopotentials the expression proposed by Williamson *et al.*,[16]

$$V_\alpha(r-R_{n\alpha}) = v_\alpha(r-R_{n\alpha})[1+\delta v_{n\alpha}(\epsilon)] = \frac{1}{\omega_c}\left(\sum_{\mathbf{q}} e^{i\mathbf{q}\cdot(r-R_{n\alpha})} v_\alpha(|\mathbf{q}|)\right)[1+\delta v_{n\alpha}(\epsilon)], \tag{A1}$$

where $v_\alpha(|\mathbf{q}|)$ has the functional form[16]

$$v_\alpha(|\mathbf{q}|) = a_{0\alpha}\frac{q^2-a_{1\alpha}}{a_{2\alpha}e^{a_{3\alpha}q^2}-1} \tag{A2}$$

and

$$\delta v_{n\alpha}(\epsilon) = \gamma_\alpha(\epsilon_{xx}+\epsilon_{yy}+\epsilon_{zz}). \tag{A3}$$

Here ϵ_{ii} are elements of the local strain tensor. The term $\delta v_{n\alpha}(\epsilon)$ plays a crucial role in describing the absolute hydrostatic deformation potentials, in particular the variation of the valence band edge and, separately, the conduction band edge under arbitrary strains. This allows us to describe the modification of the valence and conduction band offsets when the systems are subjected to hydrostatic or biaxial deformation conditions such as in the case of epitaxial growth on a lattice-mismatched substrate. Note that, even though the binary GaSb and InAs systems are nearly lattice matched (the lattice mismatch is relatively small, 0.6%), the quaternary systems manifest at the interface also Ga-As and In-Sb bonds which have a huge mutual lattice mismatch of 14% and are also strongly mismatched (by about 6%–7%) with respect to the Ga-Sb and In-As bonds. To improve the de-

TABLE III. Band parameters obtained from the pseudopotential band structure and the target band parameters of the fit. The "Target values" are conventional bulk parameters used in the literature (see Ref. 1). ΔE_{VBO} is the valence band offset relative to the target value for bulk InAs. Δ_0 is the spin-orbit splitting, m^* are the effective masses at Γ, and a_g, a_v, and b are the hydrostatic deformation potential for the band gap, the valence band maximum, and the biaxial deformation potential of the valence band, respectively.

Parameters	GaSb		InAs		GaAs		InSb	
	PP	Target	PP	Target	PP	Target	PP	Target
E_g (eV)	0.812	0.811	0.411	0.410	1.515	1.519	0.235	0.235
ΔE_{VBO} (eV)	0.544	0.540	−0.003	0.000	−0.070	−0.065	0.500	0.500
Δ_0 (eV)	0.752	0.752	0.389	0.390	0.340	0.340	0.801	0.810
m_e^*	0.039	0.042	0.022	0.024	0.059	0.067	0.015	0.014
$m_{hh}^*(001)$	0.268	0.267	0.400	0.341	0.318	0.400	0.311	0.230
$m_{hh}^*(111)$	0.676	0.780	1.051	0.917	0.814	0.900	0.220	0.476
$m_{lh}^*(001)$	0.047	0.050	0.028	0.027	0.080	0.082	0.016	0.016
$m_{lh}^*(111)$	0.042	0.045	0.026	0.026	0.070	0.080	0.011	0.015
$m_{so}^*(001)$	0.148	0.136	0.099	0.085	0.159	0.154	0.128	0.100
a_g	−7.77	−8.01	−5.56	−6.6	−8.59	−8.33	−6.16	−7.7
a_v	−1.29	−1.32	−0.92	−1.0	−1.18	−1.21	−1.03	−1.10
b	−2.16	−2.00	−1.75	−1.70	−2.07	−2.00	−2.21	−2.00

TABLE IV. Parameters of the pseudopotential for InAs, GaSb, GaAs and InSb. The potentials are fit to a plane-wave kinetic energy cutoff of 5 Ry.

Parameter	In (InAs)	In (InSb)	As (InAs)	As (GaAs)	Ga (GaAs)	Ga (GaSb)	Sb (GaSb)	Sb (InSb)
γ_α	1.3544	1.1116	0.0000	0.0000	1.8935	1.8732	0.0000	0.0000
$a_{0\alpha}$	53.5118	182.2310	66.0185	17.8028	652879.2491	1224370.2905	47.8551	92.3191
$a_{1\alpha}$	1.8990	1.7274	2.7417	2.9501	2.1456	2.0574	2.3236	2.2317
$a_{2\alpha}$	1.9048	3.4036	1.6206	1.1718	20184.1270	36491.4983	1.3224	1.6556
$a_{3\alpha}$	0.4416	0.5593	0.5934	0.3100	0.3650	0.3270	0.5248	0.6910

scription of the Ga-As and In-Sb interface bonds we have here derived the pseudopotentials with an approach slightly different from that of Ref. 1. Instead of forcing the atomic pseudopotential of a given atom to be the same in different binary compounds (i.e., Ga in GaSb and GaAs), we have allowed here the atomic potentials to be slightly different in the different compounds, to take into account the different charge redistributions and bonding properties occurring around a given ion when it is placed into a different environment. This larger flexibility of the pseudopotentials improves the description of the potential of the interface region, leading to better predictions of the electronic properties of short period SL's and alloys. The parameters entering Eqs. (A2) and (A3) have been determined by fitting, for the four *binary* systems, the experimentally measured electron and hole effective masses, band gaps (target values at 0 K), and spin-orbit splittings, hydrostatic deformation potentials of the band gaps, band offsets, and LDA-predicted single-band-edge deformation potentials.[17] In Eq. (3) the term β has been introduced to represent the quasiparticle nonlocal self-energy effects.[5] This kinetic energy scaling is needed to simultaneously fit bulk effective masses and band gaps.

In Table III we report the target values we aim to fit for the four binary compounds GaSb, InAs, GaAs, and InSb and the results of the fitting procedure. The target values correspond to the band parameters used in the literature[18] at $T=0$ K. The hydrostatic deformation potentials of the valence band maximum have been calculated using an *ab initio* LDA-based, all-electron, linearized augmented plane wave (LAPW) method.[17] A 5 Ry kinetic cutoff was used when generating the pseudopotentials and also in all the following calculations which have used the newly generated empirical pseudopotentials. From Table III we see that all the band paramaters have been fitted well. The corresponding parameters of the empirical pseudopotentials [Eq. (A2)] are given in Table IV. Although we fitted only a few band energies per material, this fit works for the full band structure. In Table V we give the results for the energies at the critical points. Where possible our calculated values are compared with the available experimental values.[11,18] The critical point energies

TABLE V. Critical point energies of bulk GaSb, InAs, GaAs, and InSb as obtained in the present relativistic EPM compared with the experimental results of Refs. 11 and 18.

States	GaSb		InAs		GaAs		InSb	
	Calc.	Expt.	Calc.	Expt.	Calc.	Expt.	Calc.	Expt.
Γ_{7v}	−0.752	−0.749/−0.82	−0.389	−0.38	−0.340	−0.341	−0.810	−0.803
Γ_{8v}	0.000	0.000	0.000	0.000	0.000	0.000	0.000	0.000
Γ_{6c}	0.812	0.811	0.411	0.410/0.418	1.515	1.519	0.235	0.235
Γ_{7c}	3.334	3.19	4.726	4.39	4.709	4.53	3.348	3.37
X_{6v}	−2.960	−3.10	−2.343	−2.4	−2.935	−2.88	−2.471	−2.4
X_{7v}	−2.704	−2.86	−2.321	−2.4	−2.852	−2.80	−2.267	−2.4
X_{6c}	1.228	1.24	2.321		1.985	1.98	1.813	1.79
X_{7c}	1.564	1.40/1.50	2.450		2.206	2.35	1.814	
L_{6v}	−1.527	−1.55	−1.102	−0.9	−1.295	−1.42	−1.412	−1.4
$L_{4,5v}$	−1.105	−1.10	−0.847	−0.9	−1.096	−1.20	−0.901	−0.9
L_{6c}	0.933	0.897/1.10	1.558		1.960	1.85	0.983	
L_{6c}-Γ_{6c}	0.121	0.084/0.10	1.147		0.445		0.748	
X_{6c}-Γ_{6c}	0.416	0.30/0.43	1.910		0.470	0.47	1.578	
X_{6c}-L_{6c}	0.295		0.763		0.025	0.17	0.830	
Δ_0'	0.257		0.486		0.194	0.17	0.487	
Δ_1	0.423	0.43/0.45	0.255	0.267	0.199		0.511	
Δ_2	0.256		0.022		0.083	0.077	0.204	
Δ_2'	0.336		0.129		0.221	0.40	0.001	

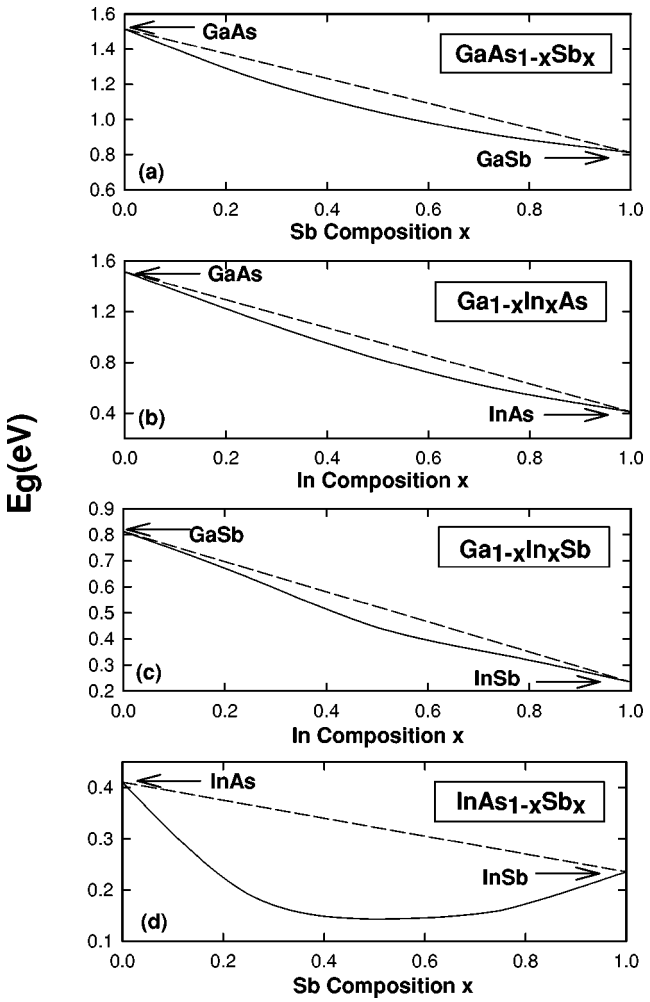

FIG. 12. Calculated fundamental gaps of the ternary (a) $GaAs_{1-x}|rmSb_x$, (b) $Ga_{1-x}In_xAs$, (c) Ga_{1-x},In_xSb, and (d) $InAs_{1-x}Sb_x$ alloys vs composition x.

and gaps of the four binary compounds are in excellent agreement with the experimental data.

Having determined the parameters of the atomic pseudpotentials we are able now to solve Eq. (3) for all the quaternary structures containing Ga, In, Sb, and As. When describing true quaternary systems we need to apply our scheme to

TABLE VI. Bowing parameter of the ternary alloys $A_{0.5}B_{0.5}C$ formed by atoms Ga, In, As, and Sb. The energy gap E_g of the alloys are calculated for a single configuration of a 512-atom unit cell whose sites were occupied randomly.

Alloy	Bowing parameter	
	PP	Expt.
$In_{0.5}Ga_{0.5}As$	0.54	0.49,[a] 0.61[b]
$In_{0.5}Ga_{0.5}Sb$	0.32	0.42[b]
$InAs_{0.5}Sb_{0.5}$	0.72	0.67,[c] 0.76[b]
$GaAs_{0.5}Sb_{0.5}$	0.53	1.0,[b] 1,43[c]

[a]Reference 16.
[b]Reference 18.
[c]Reference 11.

TABLE VII. Input parameters for the Valence Force Field calculation.

Bond	d_0(Å)	α (N/m)	β (N/m)
In-Sb	2.805	26.61	4.2842
Ga-Sb	2.640	33.16	7.2289
In-As	2.622	35.18	5.4881
Ga-As	2.448	41.19	8.9382

different atomic local environments than those present in the fitted pure binary compounds. We address the problem considering only the nearest-neighbor environment. In the quaternary $(AC)(BD)$ systems, the C and D anions can be surrounded by A_nB_{4-n} cations, where $n=0$, 1, 2, 3, and 4. Analogously, the A and B cations can be surrounded by C_nD_{4-n} anions. Our pseudopotential has been obtained by fitting the properties of only the pure binary compounds (corresponding to environments $n=0$ and $n=4$). To extend the description to the other cases, we assume a linear interpolation between these limits as

$$v_A(C_nD_{4-n})=\frac{n}{4}v_A(AC)+\frac{4-n}{4}v_A(AD),$$

$$v_B(C_nD_{4-n})=\frac{n}{4}v_B(BC)+\frac{4-n}{4}v_B(BD),$$

$$v_C(A_nB_{4-n})=\frac{n}{4}v_C(AC)+\frac{4-n}{4}v_C(BC),$$

$$v_D(A_nB_{4-n})=\frac{n}{4}v_D(AD)+\frac{4-n}{4}v_D(BD). \qquad \text{(A4)}$$

AC, BC, AD, and BD are the four binary compounds, in our case GaSb, GaAs, InSb, and InAs, whose properties have been directly fitted to extract the atomic pseudopotential parameters.

We next test the performance of the empirical pseudopotentials in the description of the electronic properties of the ternary random $In_xGa_{1-x}As$, $In_xGa_{1-x}Sb$, $GaAs_{1-x}Sb_x$, and $InAs_{1-x}Sb_x$ alloys. The random alloys are modeled by occupying randomly the sites of a 512-atom cubic supercell. We have considered only one configuration for compositions $x=0.25$, 0.50, and 0.75. For each alloy configuration, the atomic positions were relaxed using the VFF method,[19] while the supercell size is determined by a lattice constant given by the composition average of the lattice constants of the consitutent binary compounds (Vegard's law). The calculated $E_g^{alloy}(x)$ are plotted in Fig. 12. We see that the optical band bowings are always positive, and in the case of the $InAs_{1-x}Sb_x$ ternary alloy, we find the absolute minimum gap around $x=0.5$ in good agreement with experiment.[11,18]

The calculated values of the alloy bowing parameter are only indicative as they are relative to only one single configuration of the alloy and are given in Table VI for $x=0.5$. An average over many more randomly generated configurations would be needed to obtain accurate results to compare with the experiment. The agreement with the experiment is

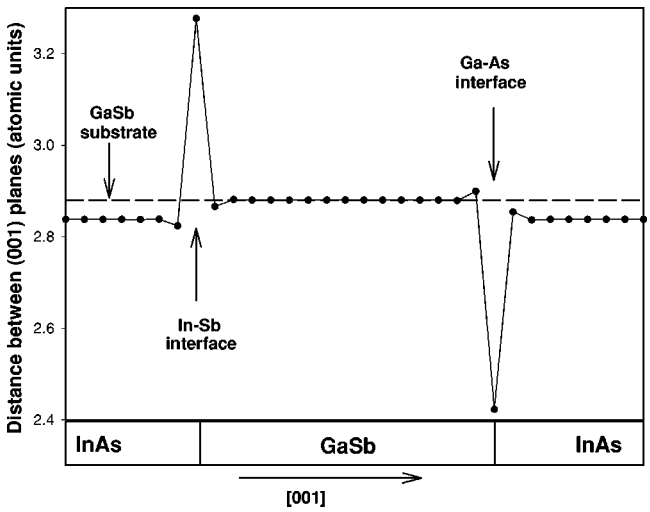

FIG. 13. Valence force field predicted interplane distances along the [001] direction in the $(InAs)_8/(GaSb)_8$ superlattice with abrupt interfaces. The distance between (001) planes in bulk GaSb is shown for reference with a dashed line.

nevetheless good. The deviations are within 0.1 for $In_{0.5}Ga_{0.5}As$, $In_{0.5}Ga_{0.5}Sb$, and $InAs_{0.5}Sb_{0.5}$. Only for the $GaAs_{0.5}Sb_{0.5}$ alloy is the calculated bowing, 0.53 eV, definetely smaller than the experimental value >1.0 eV.

The atomic positions are relaxed using the valence force field expression

$$E=\sum_i \frac{3}{8\,d_{0i}^2}\alpha_i(\mathbf{r}_i\cdot\mathbf{r}_i-d_{0i}^2)^2 \times\sum_{i,j}\frac{3}{8\,d_{0i}^2 d_{0j}^2}\beta_{i,j}\left(\mathbf{r}_i\cdot\mathbf{r}_j+\frac{1}{3}d_{0i}^2 d_{0j}^2\right)^2. \quad \text{(A5)}$$

In this expression the first sum runs over all the distinct nearest-neighbor bonds i while the second sum is over all the bonding angles formed by bonds i and j. These two terms represent the cost of bond length and bond angle distorsions. Table VII provides the bond stretching (α_i), bond bending ($\beta_{i,j}$), and ideal bond length (d_{0i}) values used for the InAs/GaSb system. The bond bending parameters $\beta_{i,j}$ for mixed In-As-Ga bonds or As-Ga-Sb bonds are calculated assuming $\beta_{In\text{-}As\text{-}Ga}=1/2\beta_{In\text{-}As\text{-}In}+1/2\beta_{Ga\text{-}As\text{-}Ga}$ and $\beta_{In\text{-}As\text{-}In}=\beta_{As\text{-}In\text{-}As}$. As an example we plot in Fig. 13 the distances between consecutive (001) planes in a $(InAs)_8/(GaSb)_8$ superlattice with abrupt interfaces obtained with the valence force field model. We can see that the distance is maximum for the In-Sb interface and minimum for the Ga-As interface, whereas in the InAs coherently strained layer the interplane distances are smaller than in the GaSb layer (lattice matched to the GaSb substrate). The resulting unit cell is slightly compressed along the [001] direction.

[1] L.W. Wang, S.-H. Wei, T. Mattila, A. Zunger, I. Vurgaftman, and J.R. Meyer, Phys. Rev. B **60**, 5590 (1999).

[2] J.R. Meyer, L.J. Olafsen, E.H. Aifer, W.W. Bewley, C.L. Felix, I. Vurgaftman, M.J. Yang, L. Goldberg, D. Zhang, C.H. Lin, S.S. Pei, and D.H. Chow, IEE Proc.-J: Optoelectron. **145**, 275 (1998).

[3] J. Steinshnider, M. Weimer, R. Kaspi, and G.W. Turner, Phys. Rev. Lett. **85**, 2953 (2000); J. Steinshnider, J. Harper, M. Weimer, C.H. Lin, S.S. Pei, and D.H. Chow, *ibid.* **85**, 4562 (2000).

[4] R. Magri and A. Zunger, Phys. Rev. B **62**, 10 364 (2000).

[5] R. Magri, L.W. Wang, A. Zunger, I. Vurgaftman, and J.R. Meyer, Phys. Rev. B **61**, 10 235 (2000).

[6] D. Gershoni, C.H. Henry, and G.A. Baraff, IEEE J. Quantum Electron. **29**, 2433 (1993).

[7] O. Krebs and P. Voisin, Phys. Rev. Lett. **77**, 1829 (1996).

[8] R. Magri and S. Ossicini, Phys. Rev. B **58**, R1742 (1998); **63**, 165303 (2001).

[9] R.G. Dandrea, C.B. Duke, and A. Zunger, J. Vac. Sci. Technol. B **10**(4), 1744 (1992).

[10] M.J. Yang, W.J. Moore, B.R. Bennet, and B.V. Shanabrook, Electron. Lett. **34**, 270 (1998); M.J. Yang, W.J. Moore, B.R. Bennet, B.V. Shanabrook, J.O. Cross, W.W. Bewley, C.L. Felix, I. Vurgaftman, and J.R. Meyer, J. Appl. Phys. **86**, 1796 (1999).

[11] I. Vurgaftman, J.R. Meyer, and L.R. Ram-Mohan, J. Appl. Phys. **89**, 5815 (2001).

[12] B.R. Bennett, B.V. Shanabrook, R.J. Wagner, J.L. Davis, J.R. Waterman, and M.E. Twigg, Solid-State Electron. **37**, 733 (1994).

[13] D.M. Wood and A. Zunger, Phys. Rev. B **53**, 7949 (1996).

[14] L.W. Wang and A. Zunger, Phys. Rev. B **51**, 17 398 (1995).

[15] J.P. Perdew and A. Zunger, Phys. Rev. B **23**, 5048 (1981).

[16] A.J. Williamson, J. Kim, L.W. Wang, S.-H. Wei, and A. Zunger, cond-mat/9805051 (unpublished).

[17] S.-H. Wei and A. Zunger, Appl. Phys. Lett. **72**, 2011 (1998).

[18] *Semiconductors: Group IV and III-V Compounds*, edited by O. Madelung, Landolt-Börnstein, New Series, Group III, Vol. 17 (Springer, Berlin, 1982); *Semiconductors: Intrinsic Properties of Group IV Elements and III-V, II-VI and I-VII Compounds*, edited by O. Madelung, Landolt-Börnstein, New Series, Group III, Vol.22 (Springer, Berlin, 1987).

[19] P. Keating, Phys. Rev. **145**, 637 (1966).

[20] L.W. Wang and A. Zunger, J. Chem. Phys. **100**, 2394 (1994).

[21] G.C. Dente and M.L. Tilton, J. Appl. Phys. **86**, 1420 (1999).

[22] L.W. Wang, J. Kim, and A. Zunger, Phys. Rev. B **59**, 5678 (1999).

[23] M.J. Shaw, E.A. Corbin, M.R. Kitchin, J.P. Hagon, and M. Jaros, J. Vac. Sci. Technol. B **18**, 2088 (2000).

[24] M.J. Shaw, Phys. Rev. B **61**, 5431 (2000).

[25] M.J. Yang, C.H. Yang, B.R. Bennet, and B.V. Shanabrook, Phys. Rev. Lett. **78**, 4613 (1997).

[26] R. Kaspi, C. Moeller, A. Ongstad, M.L. Tilton, D. Gianardi, G. Dente, and P. Gopaladasu, Appl. Phys. Lett. **76**, 409 (2000); A.P. Ongstad, R. Kaspi, C.E. Moeller, M.L. Tilton, D.M. Gianardi, J.R. Chavez, and G.C. Dente, J. Appl. Phys. **89**, 2185 (2001).

[27] O. Dehaese, X. Wallart, and F. Mollot, Appl. Phys. Lett. **66**, 52 (1995).

[28] B. Koiller, R.B. Capaz, and H. Chacham, Phys. Rev. B **60**, 1787 (1999).

[29] R. Magri and A. Zunger, Phys. Rev. B **64**, R081305 (2001).
[30] J. Harper, M. Weimer, D. Zhang, C.-H. Lin, and S.S. Pei, Appl. Phys. Lett. **73**, 2805 (1998).
[31] M. Weimer (private communication).
[32] R.M. Feenstra, D.A. Collins, D.Z.Y. Ting, M.W. Wang, and T.C. McGill, Phys. Rev. Lett. **72**, 2749 (1994).
[33] M.E. Twigg, B.R. Bennett, P.M. Thibado, B.V. Shanabrook, and L.J. Whitman, Philos. Mag. A **7**, 7 (1998).